The Astrophysical Journal, 961:241 (17pp), 2024 February 1 https://doi.org/10.3847/1538-4357/ad0cc2
© 2024. The Author(s). Published by the American Astronomical Society.
OPEN ACCESS

Compact Symmetric Objects. II. Confirmation of a Distinct Population of High-luminosity Jetted Active Galaxies

S. Kiehlmann[1], A. C. S. Readhead[2], S. O'Neill[2], P. N. Wilkinson[3], M. L. Lister[4], I. Liodakis[5,6], S. Bruzewski[7], V. Pavlidou[1,8], T. J. Pearson[2], E. Sheldahl[7], A. Siemiginowska[9], K. Tassis[1,8], and G. B. Taylor[7]
[1] Institute of Astrophysics, Foundation for Research and Technology-Hellas, GR-70013 Heraklion, Greece
[2] Owens Valley Radio Observatory, California Institute of Technology, Pasadena, CA 91125, USA; acr@caltech.edu
[3] Jodrell Bank Centre for Astrophysics, University of Manchester, Oxford Road, Manchester M13 9PL, UK
[4] Department of Physics and Astronomy, Purdue University, 525 Northwestern Avenue, West Lafayette, IN 47907, USA
[5] Finnish Center for Astronomy with ESO, University of Turku, Vesilinnantie 5, FI-20014, Finland
[6] Department of Physics, University of Crete, GR-70013 Heraklion, Greece
[7] Department of Physics and Astronomy, University of New Mexico, Albuquerque, NM 87131, USA
[8] Department of Physics and Institute of Theoretical and Computational Physics, University of Crete, GR-70013 Heraklion, Greece
[9] Center for Astrophysics | Harvard & Smithsonian, 60 Garden Street, Cambridge, MA 02138, USA
Received 2023 March 20; revised 2023 October 16; accepted 2023 November 4; published 2024 January 31

Abstract

Compact symmetric objects (CSOs) are compact (<1 kpc), jetted active galactic nuclei (AGN), whose jet axes are not aligned close to the line of sight, and whose observed emission is not predominantly relativistically boosted toward us. Two classes of CSOs have previously been identified: approximately one-fifth are edge dimmed and the rest are edge brightened. We designate these as CSO 1s and 2s, respectively. This paper focuses almost exclusively on CSO 2s. Using complete samples of CSO 2s we present three independent lines of evidence, based on their relative numbers, redshift distributions, and size distributions, which show conclusively that the vast majority (>99%) of CSO 2s do not evolve into larger-scale radio sources. These CSO 2s belong to a distinct population of jetted AGN, which should be characterized as "short-lived," as opposed to "young," compared to the classes of larger jetted AGN. We show that there is a sharp upper cutoff in the CSO 2 size distribution at ≈500 pc. The distinct differences between most CSO 2s and other jetted AGN provides a crucial new time domain window on the formation and evolution of relativistic jets in AGN and the supermassive black holes that drive them.

Unified Astronomy Thesaurus concepts: Active galactic nuclei (16); Active galaxies (17); Relativistic jets (1390)

Supporting material: machine-readable table

1. Introduction

The first indication of relativistic motion in the jets of active galaxies was the asymmetric large-scale jet in M87 discovered by Curtis (1918). The next was arguably the discovery of rapid flux density variations in blazars (Dent 1965a, 1965b), which were quickly shown by Rees (1966, 1967) to be due to relativistic motion of the emission regions toward the observer. In spite of this development, observations of the synchrotron self-absorption cutoff frequencies of radio sources with flat spectra led to the hypothesis that an "inverse Compton catastrophe" imposes an upper limit of $\sim 10^{12}$ K on the brightness temperatures of compact radio sources (Kellermann & Pauliny-Toth 1969). This appeared, at first, to be supported by very long baseline interferometry (VLBI) observations, but in these calculations the possibility of relativistic bulk motion toward the observer (Rees 1966, 1967) was not taken into account.

The first phase-coherent astronomical image ever obtained in any energy band, including the optical band, having a resolution significantly less than 1″ was produced in the first "hybrid map," which showed an asymmetric one-sided radio jet (Wilkinson et al. 1977). Such core–jet structures were soon shown to predominate in compact radio sources (Readhead et al. 1978; Readhead 1980), making it clear that relativistic beaming determines the apparent morphology and the observed brightness temperatures of most compact radio sources at centimeter wavelengths. Nevertheless, the inverse Compton catastrophe hypothesis continued to propagate, but, as shown by Readhead (1994), when relativistic beaming is taken into account, the brightness temperatures drop to $\sim 10^{11}$ K, and are consistent with equipartition between the magnetic field and particle energy densities in the emission regions.

It should therefore be clear that relativistic beaming greatly complicates the physical analysis of the observed radio emission of compact radio sources. In order to overcome such complications, which introduce large uncertainties in the physical properties, such as the magnetic field strength, the particle energy densities, the pressures, and the total energies of the emission regions, Wilkinson et al. (1994, hereafter W94), introduced the compact symmetric object (CSO) classification of compact radio sources. Due to the morphological symmetry of the emission on either side of the nucleus, these objects are clearly not exhibiting strongly beamed emission toward the observer.

Unfortunately, a number of jetted active galactic nuclei (AGN) have been misidentified as CSOs or CSO candidates in the literature, and many jetted AGN whose axes are close to the line of sight, and whose observed emission is strongly beamed toward us, have crept into this class. This paper is the second of three on the morphological radio properties of CSOs in which we explore CSO phenomenology uncontaminated by objects

Original content from this work may be used under the terms of the Creative Commons Attribution 4.0 licence. Any further distribution of this work must maintain attribution to the author(s) and the title of the work, journal citation and DOI.

that have been misidentified as CSOs. In Paper I (Kiehlmann et al. 2024) we added two new criteria, based on variability and speed, to the CSO selection criteria and undertook a detailed survey of the literature, which enabled us to identify 79 bona fide CSOs. From the 79 bona fide CSOs we determined the numbers in three complete samples[10] from which, in this paper (Paper II), we show that $\gtrsim$99% of CSO 2s form a class of jetted AGN that is both distinct from other jetted AGN and exhibits a sharp cutoff in size at $\approx$500 pc, and a corresponding cutoff in age at $\approx$5000 yr, so that only fewer than 1% of CSO 2s might possibly go on to form the larger classes of jetted AGN, such as Fanaroff and Riley Type I (FR I) and Type II (FR II) objects (Fanaroff & Riley 1974). In Paper III (Readhead et al. 2024) we discuss the evolution of CSO 2s and show that while they are nearly all "short-lived" compared to the classes of larger jetted AGN, only a minority of them are "young." Note that FR I and FR II objects have sizes in the $\sim$20 kpc to several megaparsecs range, and therefore clearly have ages much longer than the vast majority of CSO 2s. We should avoid the implicit assumptions involved in calling all CSO 2s "young," which obscure the true nature and importance of this class of jetted AGN. It is critically important, therefore, to recognize the distinction between the terms "young" and "short-lived," which otherwise obfuscate the phenomenology of the CSO class.

In an important development in the study of CSOs, Tremblay et al. (2016) showed that there are two major morphological classes of CSOs: edge-dimmed objects, which we designate as CSO 1s, and edge-brightened objects, which we designate as CSO 2s. Paper I confirms their finding and this paper deals almost exclusively with CSO 2s.

As discussed in detail in Paper I, in CSOs, two emission regions are seen straddling the center of activity, making it clear that these cannot be strongly relativistically boosted, otherwise the object would be seen as a one-sided asymmetric "core–jet" object as is the case in the vast majority of compact radio sources observed at centimeter wavelengths (Kellermann et al. 1998; Lister et al. 2019).

Individual CSO 2s undergo appreciable evolutionary structural changes on timescales of years that can therefore be studied without the complications of relativistic beaming. The bulk flows along their jets and their speeds of advance into the interstellar medium can be measured directly. We argue that CSO 2s provide a uniquely accessible time domain laboratory for the study of relativistic jets (Blandford et al. 2019) and the supermassive black hole (SMBH) central engines that drive them, because they are short-lived compared to the classes of larger jetted AGN, rather than young, and hence pass through all stages of their lives as CSO 2s, which are therefore available for detailed study in all phases of their lives. It is important to distinguish between CSOs that have small sizes because they are "short-lived" compared to larger classes of jetted AGN, and CSOs that have been stalled by the interstellar medium of their host galaxies and therefore stopped growing in size. We propose the hypothesis that such stalled CSOs are likely to be edge dimmed and hence fall into the CSO 1 class. We also note in passing that this could be of great importance to feedback. As we show in Paper III, the most luminous CSOs are CSO 2s. These are the subject of this study, and they have not been stalled—their hot spots are separating on average by $\sim$0.4c, and their maximum lifetimes are $\sim$5000 yr. For the purposes of this study, although stalled CSOs are of great potential interest, we do not consider them further in these three papers. A minority of the less luminous CSOs in our study might possibly be stalled systems and should also be considered in that light. But this is beyond the scope of the present study.

By the early 1990s, three bona fide CSO 2s had been definitively identified in the complete sample of 65 radio sources studied by Pearson & Readhead (1988). Despite the small size of the CSO sample, and entirely because it was part of a complete sample, this sample of only three CSO 2s was enough to enable a number of the most critical questions about CSO 2s to be addressed by Readhead et al. (1994, hereafter R94), including their relationship to the larger jetted AGN, their lifetimes, and their energy requirements. R94 concluded that CSO 2s form a distinct population of compact jetted AGN, and that there must be a physical reason for this which provides a unique window on the central engines that drive AGN. R94 also suggested that CSO 2s might be the result of the capture of a single star by an SMBH in an otherwise quiescent elliptical galaxy nucleus. This possibility was also suggested more recently by An & Baan (2012).

All of these properties of CSO 2s were discussed in more detail, and confirmed, in Readhead et al. (1996, hereafter R96). Nevertheless, in spite of their distinction, CSO 2s have attracted comparatively little attention among jetted AGN enthusiasts. We explore the characteristics of CSO 2s in considerably more detail in this paper and in Paper III.

CSOs are a subset of AGN, but by studying a restricted well-defined sample of CSOs we aim to understand them in depth and gain new insights into the physics and formation of jetted AGN in general. Although it is not a primary goal of these papers, we discuss the relationship of CSOs to other classes of AGN where appropriate in this paper and in Paper III. To place CSOs in the broader context of compact radio sources associated with AGN, the reader is referred to the comprehensive review of O'Dea & Saikia (2021, hereafter OS21).

Throughout this paper we adopt the convention $S_\nu \propto \nu^\alpha$ for spectral index α, and use the cosmological parameters $\Omega_m = 0.27$, $\Omega_\Lambda = 0.73$, and $H_0 = 71$ km s^{-1} Mpc^{-1} (Komatsu et al. 2009). We do this for consistency with our other papers. None of the conclusions would be changed were we to adopt the best model of the Planck Collaboration (Planck Collaboration et al. 2020).

2. Complete Samples of Jetted AGN

The disposition of the CSOs we consider in this study, among the CSO 1 and CSO 2 classes, the CSOs with spectroscopic redshifts and those without, and the CSOs in the complete samples is shown in Table 1. The classification of CSO 1s and CSO 2s that we use here is discussed in more detail in Paper III.

We use only complete samples for the statistical tests in this paper. Other methods for making statistical tests, which are not based on complete samples, must introduce some assumptions regarding the population under study, and we wish to avoid making such assumptions. We use three complete samples extensively (see Table 2): (1) the 5 GHz Pearson–Readhead (PR) complete sample (Pearson & Readhead 1988) based on the MPIfR/NRAO S4 and S5 surveys (Pauliny-Toth et al. 1978; Kuehr et al. 1981); (2) the first Caltech–Jodrell (CJ1) 5 GHz complete sample (Polatidis et al. 1995; Xu et al. 1995)l;

[10] A "complete sample" is defined to be a sample that includes all objects down to a given flux density limit over a given area of sky (Pooley & Ryle 1968; Schmidt 1968; Longair & Scheuer 1970).

Table 1
The CSO Samples

	CSO 1	CSO 2	All
With spectroscopic redshifts	11	43 (17)	54
Without spectroscopic redshifts	5	20 (2)	25
All	16	63 (19)	79

Note. This table shows the numbers of bona fide CSOs of classes 1 and 2 identified in Paper III, with and without spectroscopic redshifts. Numbers in parentheses indicate bona fide CSOs in the PR+CJ1+PW complete samples. In this paper we deal almost exclusively with the 17 CSOs in these complete samples that have spectroscopic redshifts.

and (3) the Peacock–Wall (PW) 2.7 GHz complete sample (Peacock & Wall 1981; Wall & Peacock 1985).[11]

There are 282 objects in the union of these three complete samples and these are listed in Table A1 in the Appendix. In our analysis in this paper, we exclude M82 (3C 231) which is in the PR and PW samples, but is a starburst galaxy and not a jetted AGN, leaving 281 sources. In Paper I we listed the number of CSOs in the three complete samples. The number of CSO 2s in each of these three complete samples is given in Table 2. The determination of a uniform set of measurements of the largest angular size of the 79 bona fide CSOs is described in Paper I.

All the sources in the PW sample were mapped using the Cambridge 5 km Telescope by Peacock & Wall (1981), who also classified the large-scale structures in the PW sample according to the following types: (i) FR I, FR II, and an intermediate FR type (FR?); (ii) objects unresolved on the 5 km Telescope (U); (iii) compact steep spectrum (CSS) objects having $\alpha \leqslant -0.5$ between 2.7 GHz and 5 GHz; and (iv) double objects with the optical identification coincident with one of the two radio components. These types are listed in column (7) of Table A1 in the Appendix.

Discussions of a size cutoff in CSO 2s are not new (Augusto et al. 1998, 2006; Augusto 2009), and early lobe-speed measurements showed that the hot spots of CSO 2s are rapidly separating (Owsianik & Conway 1998; Owsianik et al. 1999; Polatidis et al. 2002). It was clear, therefore, as pointed out in R94 and R96, that CSO 2s must be short-lived, since otherwise there would be far more of their longer-lived, larger counterparts. This means that CSO 2s *must* exhibit a size cutoff. As shown in this paper, we have now determined that a sharp cutoff occurs at ≈500 pc. The evolution of the vast majority of CSO 2s from "early life" through "midlife" to "late life" is discussed in detail in Paper III, where we also discuss the fact that a small fraction of CSO 2s almost certainly go on to form the larger classes of jetted AGN, including medium symmetric objects (MSOs), FR Is and FR IIs. We show in this paper that this fraction is <5% for MSOs, and <1% for FR Is and FR IIs.

Since the CSOs in the PR+CJ1+PW complete samples are all CSO 2s, the findings of this paper apply (i) only to CSO 2s and (ii) only to the high-luminosity end of the CSO 2 luminosity function. Much deeper complete sample surveys, in which we are engaged, are needed to expand our knowledge into the low-luminosity regime of CSO 2s. It should therefore be borne in mind that our sample, comprising only 17 objects, is small, so that a degree of caution must be exercised in interpreting the results. For this reason we present all of the relevant statistics and *p*-values so that readers may judge for themselves the significance of the results.

There are precedents in astronomy for drawing powerful conclusions based on small numbers. For example, Hubble (1929a, 1929b) based his discovery of the expansion of the Universe on measurements of just 22 galaxies. Minkowski (1941) had just 14 supernovae for his classification of Type I and Type II supernovae, with nine and five objects, respectively. Closer to the approach of this paper, there is also a powerful precedent for using well-defined statistical tests based on complete samples in the paper by Schmidt (1968), who used a complete sample of just 33 quasars to demonstrate convincingly that quasars are not evenly distributed in space, but show strong cosmological evolution.

In this paper we present three independent sets of data and lines of argument based on complete samples, each of which shows that the vast majority of CSO 2s form a distinct population of jetted AGN. These lines of argument are based on (i) the numbers of CSO 2s in complete samples, (ii) the redshift distributions of these CSO 2s, and (iii) the size distribution of these CSO 2s. Of these, the results of the first and third arguments are, in our view, compelling. The results of the second argument (ii) are significant only at the p-value $= 1.6 \times 10^{-2}$ (2.1σ) level, and are, therefore, not compelling, but they are in the same sense as the other two arguments—i.e., they strongly suggest that the CSO 2s are drawn, predominantly, from a distinct population of jetted AGN.

The PW sample was selected at 2.7 GHz, unlike the PR and CJ1 samples which were selected at 5 GHz. However, we have 5 GHz flux densities for all the PW sources (Pauliny-Toth 1977). Following a suggestion by John Peacock, in order to be able to combine results from these three complete samples without introducing any possible biases due to the different sample selection frequencies, we define a subset of the PW sample that is effectively complete at 5 GHz. For this purpose we compare the GB6 (Gregory et al. 1996), PR, and PW samples at 5 GHz over their common sky area ($35° \leqslant \delta \leqslant 75°$, $|b| \geqslant 10°$, B1950). These surveys were all made with different instruments at different times and since many of the sources are variable the samples change slightly with time. In this area of sky, the GB6 survey has 54, the PR survey has 51, and the PW survey has 54 objects with $S_{5\ \mathrm{GHz}} \geqslant 1.3$ Jy. It may safely be assumed, therefore, that the PW sample is effectively complete down to 1.3 Jy at 5 GHz. Of these we define a subsample, PWS, where "S" stands for "subsample," consisting of the PW sources at declinations $\delta < 35°$ (B1950) and having $S_{5\ \mathrm{GHz}} \geqslant 1.3$ Jy, for use in our physical size distribution statistical tests in Section 5. We point out that all of the PW CSOs at $\delta \geqslant 35°$ are in the PW+CJ1 sample.

The great strength of the PR, CJ1, and PW samples is that all of the objects are well studied and their radio properties on both large and small scales are known. There is, therefore, no danger of unknown selection bias that could compromise the statistics. In Table A1 in the Appendix we list all of the sources in the complete PR, CJ1, and PW samples and we provide references to these structure observations. Clearly, the references given in Table A1 do not include all of the papers that refer to the objects in these samples—in many cases we provide only a

[11] The original PW sample (Peacock & Wall 1981) contained 168 sources; to these three (DA 240, 0945+73 = 4C 73.08, and NGC 6251) source were added by Wall & Peacock (1985).

Table 2
The Numbers of CSS, FR I, FR II, and CSO Objects in the Complete Samples

Complete Sample	Flux Density Limits	CSS Number	FR I Number	FR II Number	Total Number	CSO 2 Number	CSO 2/FR II Percentage	CSO 2/Total Percentage
PR	$S_5 \geqslant 1.3$ Jy	6	3	16	64[a]	6	37.5% ± 18.0%	9.4% ± 4.0%
CJ1	1.3 Jy $\geqslant S_5 \geqslant 0.7$ Jy	23	6	30	135	6[b]	20.0% ± 8.9%	4.4% ± 1.9%
PR+CJ1	$S_5 \geqslant 0.7$ Jy	29	8	46	199[a]	12[b]	26.1% ± 8.5%	6.0% ± 1.8%
PW	$S_{2.7} \geqslant 1.5$ Jy	26	15	65	170[a]	13[c]	20.0% ± 6.1%	7.6% ± 2.2%
PWS	$S_5 \geqslant 1.3$ Jy	7	8	11	50	5	45.5% ± 24.5%	10.0% ± 4.7%
PR+CJ1+PW	⋯	43	16	76	281[a]	19[b] [c]	25.0% ± 6.4%	6.8% ± 1.6%

Notes. All of the CSOs in the PR+CJ1+PW sample are CSO 2s. In addition, all of the PW CSOs at $\delta \geqslant 35°$ are in the PR+CJ1 sample.
[a] The numbers exclude 3C 231 (M82), a starburst galaxy, not an AGN.
[b] The numbers include the bona fide CSO J1335+5844, for which there is no published spectroscopic redshift.
[c] The numbers include the bona fide CSO J1416+3444, for which there is no published spectroscopic redshift. These numbers are taken from the list of the 282 sources in the three complete samples given in Table A1 in the Appendix. PWS is the subsample of PW at $10° < \delta < 35°$ (B1950) and with $S_{5\ \mathrm{GHz}} > 1.3$ Jy. As should be clear in view of the size of the samples, and assuming there is no dependence of the CSO fraction on flux density, the most reliable statistic is the final one combining the three full samples, PR+CJ1+PW.

single reference to a paper that contains a good map of the object.

In addition to the above three complete samples, there is one other complete sample that is of prime importance to this study: the GaLactic and Extragalactic All-Sky Murchison Widefield Array (GLEAM) survey (Callingham et al. 2017), which covers the sky area $\delta < 30°$ (J2000), $|b| > 10°$ and defines a complete sample of 11,400 objects exhibiting flux densities greater than 1 Jy in the 72–700 MHz range.

In the following sections, using the complete samples, we provide three lines of argument that the vast majority of CSO 2s form a distinct population of jetted AGN.

3. The Fractions of CSO 2s in Complete Samples

It is important to note that, in addition to the identification of 79 "bona fide" CSOs in Paper I, we also identified 167 "class A" CSO candidates, which are objects showing clear double structure, but for which the maps are not of sufficient quality to confirm them as CSO 2s. We have Very Long Baseline Array (VLBA) observations of these and are in process of analyzing them. We also identified 1164 "class B" CSO candidates, most of which are far less likely to be CSO 2s, but which cannot yet definitively be ruled out.

R96 gave a detailed discussion of the CSO fractions in the PR and CJ1 complete samples. Here we update this discussion and also incorporate the PW sample.

While the PR CSO sample is complete, as can be seen in Paper I, in CJ1 there are five class A CSO candidates which might possibly be bona fide CSO 2s. All of these candidates have sizes less than 500 pc, and, were we to include these five sources in our analysis, the conclusions below would be strengthened. We prefer to take the conservative route and not to include any CSO candidates in the bona fide sample until they have met the CSO criteria laid out in Paper I.

As can be seen in Paper I, there are also six class B CSO candidates in the PR, CJ1, and PW samples. These are much less likely to be bona fide CSO 2s, and all but one have sizes less than 500 pc. For these reasons, the conservative approach is again not to include any of these objects in the present analysis.

We see in Table 2 that the fraction of CSO 2s in the complete 2.7–5 GHz samples is $(6.8 \pm 1.6)\%$. This would rise to $(8.5 \pm 1.8)\%$ if all of the class A CSO 2s candidates in the CJ1 sample are shown to be bona fide CSOs.

We take as a simple hypothesis to be used throughout this paper, that, between their appearance and disappearance, the separation speed, v_{sep}, of the opposing hot spots in CSO 2s, when averaged over a sufficient interval of time, is constant, and that they continue at the same separation speed if they expand to form larger classes of sources, such as FR IIs. Under this hypothesis, the number of objects in different size ranges scales simply in proportion to the size ranges.

It is important to note that, for the purposes of our arguments regarding the fractions of CSO 2s with respect to classes of larger sources, this hypothesis is highly conservative. We show in Paper III that the separation speed of the hot spots for CSO 2s is $v_{\mathrm{sep}} = (0.36 \pm 0.04)c$, whereas, for example, Carilli et al. (1991) argue convincingly that for the opposing hot spots in Cygnus A, $0.01c < v_{\mathrm{sep}} < 0.05c$. Note that this deduced separation speed for Cygnus A is typical for FR IIs (Scheuer 1995). Based on these values, the separation speeds in CSO 2s are approximately an order of magnitude greater than those in FR IIs, which means that if CSO 2s do expand to form FR IIs, they spend far less of their time in the 0–1 kpc size range than under the constant speed hypothesis, and so there should be even fewer of them relative to FR IIs than under the constant speed hypothesis.

Under the constant speed hypothesis we also assume that the luminosity does not change enough for the source to drop out of the flux-limited sample. We discuss possible changes in luminosity later.

We consider three populations of objects that are larger than CSO 2s and that might, therefore, be the populations that CSO 2s evolve into:

(i) CSS objects (Peacock & Wall 1982), including the subclass of MSOs, which have sizes in the range 1–20 kpc (Fanti et al. 1995; R96). Note that MSOs have the same characteristics as CSO 2s apart from the size range.
(ii) FR I jetted AGN (Fanaroff & Riley 1974), which have sizes that range up to ≈1 Mpc—see Figure 1 (top panel).
(iii) FR II jetted AGN (Fanaroff & Riley 1974), which also have sizes that range up to ≈1 Mpc—see Figure 1 (bottom panel).

Note that Fanti et al. (1995) and R96 used an upper size limit of $15h^{-1}$ kpc for MSOs, where $H_{\mathrm{o}} = 100h$ km s^{-1} Mpc^{-1}. For our adopted cosmology, this translates to 21 kpc. However, since the original choice of $15h^{-1}$ kpc was chosen by Fanti et al. (1995) and R96 to be a convenient "round number," we

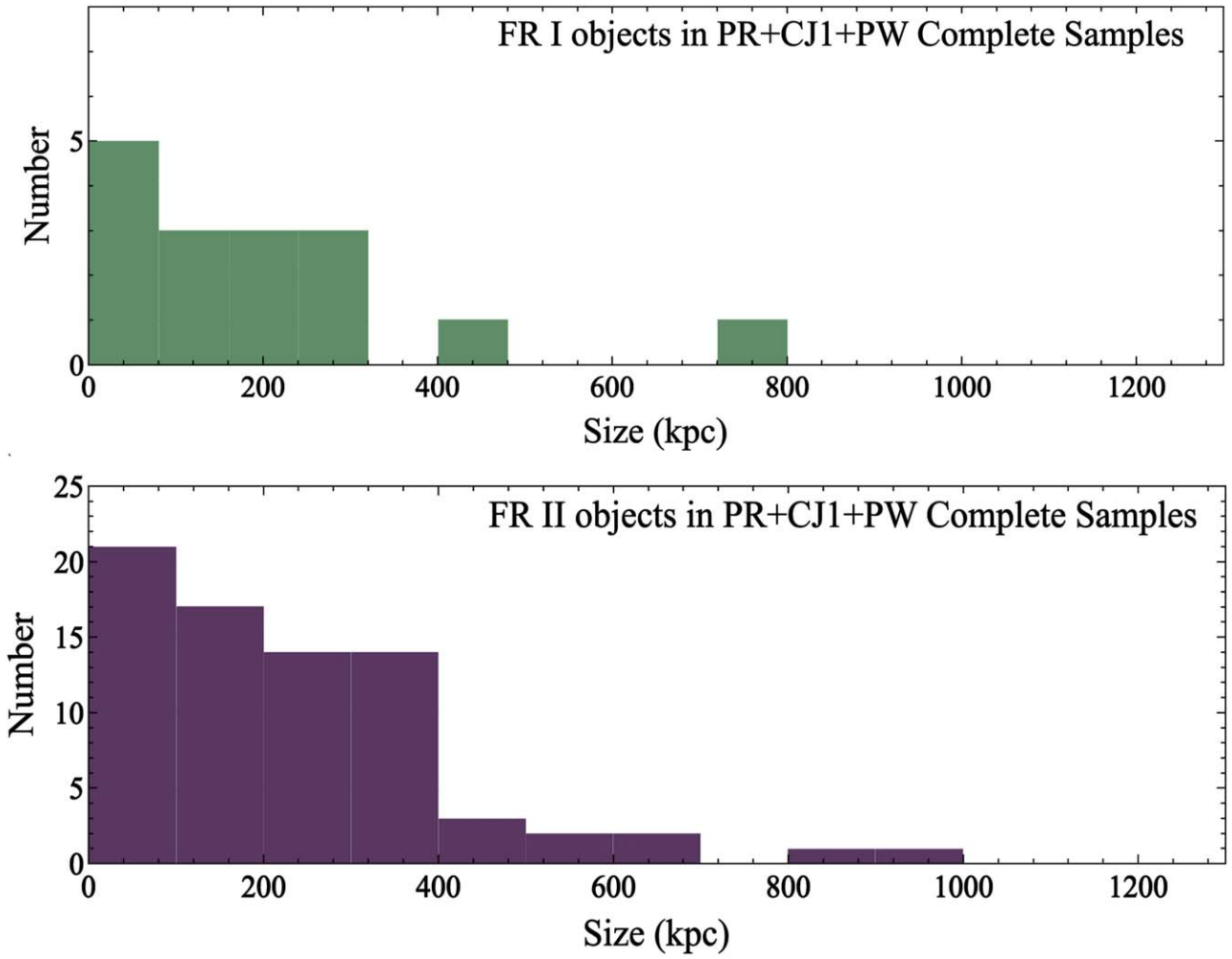

Figure 1. The distributions of the largest projected sizes of FR I objects (top panel) and FR II objects (bottom panel) in the PR+CJ1+PW complete samples. The FR I sizes have been determined from our own angular size measurements. The FR II sizes are based on the largest angular size measurements of Nilsson et al. (1993) for all but six sources not included in their sample, for which we measured the angular sizes ourselves. There is one FR II object (3C 236) of size 4.3 Mpc that is not included in the FR II plot.

will follow that practice and use 20 kpc as the upper size limit of MSOs in this study, which also accords with the upper limit on MSO and CSS sizes adopted by OS21.

The fact that the fraction of CSOs in complete samples is far too high for them all to evolve into larger classes of radio sources was first discussed by R94, and has since been much studied (see OS21). Here we discuss the results for the hona fide CSO 2s in our complete samples. We see from Table 2 that there are 19 CSO 2s and 43 CSS objects in the combined PR +CJ1+PW complete sample. Note that MSOs are a subset of the CSS class. Thus the fraction of CSO 2s in the combined CSO+CSS sample is $(30 \pm 8)\%$. Assuming an upper limit on CSS and MSO sizes of 20 kpc, on our hypothesis of constant speed of advance, the number of CSO 2s in complete samples of CSS and MSOs should be $1/20 = 5\%$. This means that the fraction of CSO 2s that evolve into MSOs is $\lesssim 5\%$. We therefore reject the hypothesis that a significant fraction of CSO 2s evolve into CSS+MSO sources.

The median size of the FR I sources in the combined PR, CJ1, and PW sample shown in Figure 1 is 180 kpc. This can be compared to the median size of the CSO 2s in these samples of 215 pc. The ratio in sizes ≈ 837, so that on the hypothesis of constant expansion speed we would expect there to be $\sim 15{,}907$ FR Is, whereas there are 16—i.e., there are $\sim 990\times$ fewer FR Is than expected. Conversely, given the number of FR Is in these three complete samples, there are $\approx 990\times$ more CSO 2s than expected.

The median size of the FR II sources in the combined PR, CJ1, and PW sample shown in Figure 1 is 305 kpc. This can be compared to the median size of the CSO 2s in these samples of 215 pc. The ratio in sizes ≈ 1420, so that on the hypothesis of constant expansion speed we would expect there to be $\sim 27{,}000$ FR IIs, whereas there are 77—i.e., there are $\sim 350\times$ fewer FR IIs than expected. Conversely, given the number of FR IIs in these three complete samples, there are $\approx 350\times$ more CSO 2s than expected.

We see therefore that the numbers of both FR I and FR II sources relative to CSO 2s are far too small, by factors of over 900 for the FR Is and over 300 for the FR IIs, for CSO 2s to evolve into either FR I or FR II sources of comparable radio luminosity. At this flux density level the integrated number flux density counts have a power-law slope of -1.3, so that the luminosity would have to drop by factors of 200 and 90, respectively, to accommodate this scenario for FR I or FR II objects.

Rawlings & Saunders (1991) have shown that there is a strong correlation between radio jet power and optical narrow line luminosity. Based on observations by Lawrence et al. (1996),

Table 3
Redshifts and Sizes of the 17 CSO 2s with Spectroscopic Redshifts in the PR, CJ1, and PW Complete Samples

IAU Name	Redshift	Size (pc)	PR	CJ1	PW
J0029+3456	0.517	180			Y
J0111+3906	0.668	56	Y		
J0119+3210	0.0602	115			Y
J0405+3803	0.05505	44		Y	
J0713+4349	0.518	217	Y		Y
J1035+5628	0.46	221	Y		Y
J1227+3635	1.975	499		Y	Y
J1244+4048	0.8135	529		Y	
J1326+3154	0.37	345			Y
J1347+1217	0.121	215			Y
J1400+6210	0.431	378	Y		Y
J1407+2827	0.077	16			Y
J1609+2641	0.473	362			Y
J1735+5049	0.835	61		Y	
J1944+5448	0.263	196		Y	
J2022+6136	0.227	104	Y		Y
J2355+4950	0.237	337	Y		Y

Note. References for the redshifts and sizes are given in Paper I.

R96 showed that the narrow line luminosities of the CSO 2s J0111+3906, J0713+4349, and J2355+4950 are about a factor 30 below that of typical FR II galaxies, so that if CSO 2s are to evolve into FR II galaxies, then their optical line luminosities must increase by about a factor 30 while their radio luminosities decrease by about a factor 35, which seems an unlikely scenario. It is interesting to note that R96 show that the jet power for J2355+4950, when corrected for the Hubble constant and different cosmologies, is $\sim 7 \times 10^{43}$ erg s^{-1}, and for J0111+3906, and J0713+4349 the similarly corrected jet powers are $\sim 10^{45}$ erg s^{-1}, which may be compared to the range of jet powers in FR II sources of $\sim 10^{44}$ erg s^{-1}–10^{47} erg s^{-1} (R96). Thus the jet powers of CSO 2s are similar to those of FR II objects, as is also the case regarding their luminosities. Given the agreement in narrow line luminosity between CSO 2s and FR I galaxies, the possible evolutionary scenario from CSO 2s to FR I galaxies may seem promising, but again, the numbers are off by over a factor 900.

We conclude on the basis of these fractions of CSO 2s in complete samples that the vast majority ($\gtrsim$95% for MSOs, and and $\gtrsim$99% for FR Is and FR IIs) of CSO 2s do not evolve into any of the above classes of larger jetted AGN, and therefore that they belong to a distinct class of jetted AGN.

4. The Redshift Distribution of the CSO 2s in the Complete Samples

An independent test of whether or not the CSO 2s are drawn from the same population as the other jetted AGN in our complete samples is provided through the redshift distribution. The redshifts are listed in Table 3. The redshift distributions of the PR+CJ1 and PW complete samples, and their corresponding CSO distributions, are shown in Figure 2.

We have carried out a Kolmogorov–Smirnov (K-S) two-sample test on the PR+CJ1 sample, the PW sample, and the PWS sample. The results of the tests are shown in Table 4. The cumulative distributions corresponding to Tests #1, #2, and #3, and their K-S statistics, are shown in Figures 3(a), (b), and (c). In carrying out these tests we have removed the CSO 2s from the full samples. The K-S statistic is completely determined by the data, but the corresponding p-value depends on the assumptions made in integrating over the parent distribution (Press et al. 1992). We verified that MATLAB and Numerical Recipes use the same formulae for determining the p-values. For that reason we use the MATLAB p-values in deriving the significance levels in Table 4.

The first two redshift distribution tests (#1 and #2 in Table 4) show that the probability of the hypothesis that the CSO 2s and non-CSO 2s are drawn from the same population is 0.13 for the PR+CJ1 sample and 0.03 for the PW sample. If we look at the effectively complete PW subsample having $S_{5\,\mathrm{GHz}} > 1.3$ Jy and at decl. $\delta < 35°$, which is independent of the PR+CJ1 sample in view of the mutually exclusive decl. limits, we see that the probability is 0.12. Since these are independent samples, we may legitimately multiply the p-values of Tests #1 and #3, which yields a probability of 1.6×10^{-2}, which is significant at the 2.1σ level. While not at the 3σ level, these statistics nevertheless provide some independent evidence that CSO 2s are drawn from a different population compared to that of the other jetted AGN in these complete samples.

This result, which is seen clearly in the redshift distributions shown in Figure 2, is interesting. If correct, it suggests that CSO 2s only started forming in significant numbers toward the end of the epoch of maximum galaxy and star formation: the lookback time to the peak in the cosmic star formation rate (SFR) is ∼8 billion years (Förster Schreiber & Wuyts 2020), which is close to the lookback time to redshift $z \approx 0.9$, when CSO 2s started to appear in significant numbers, as can be seen in Figures 2(a) and (b). The peak SFR occurs from $z \approx 1$ to $z \approx 2$, with the peak SMBH formation rate (Tacconi et al. 2020) peaking slightly after the peak SFR.

Thus, a possible explanation of the origin of CSO 2s is that quiescent SMBHs form CSO 2s by single star capture, and so become significant around $z \sim 1$, when the numbers of both stars and SMBHs in the Universe reach a maximum. We give a detailed discussion of this hypothesis in Paper III.

However results that are significant only at the $\sim 2\sigma$ level often disappear with the advent of more data, and this particular apparent difference between CSO 2s and other jetted AGN may disappear as more bona fide CSO 2s are accrued through new and deeper complete samples. An important point that should be mentioned here is that there are 14 bona fide CSOs in the VLBA Imaging and Polarization Survey (VIPS) of flat spectrum ($\alpha \geqslant -0.5$)) sources (Helmboldt et al. 2007) that are not in the complete PR+CJ1+PW samples, and of these only one has a redshift greater than 1. Thus, extending the luminosity function almost an order of magnitude deeper appears not to change our findings in this section. This gives us confidence that this preliminary 2.1σ result will be greatly strengthened, when we are able to add the steep spectrum counterparts to the VIPS survey to make this a complete sample, as we are now engaged in doing.

As a distinct population, and recalling that these are all "short-lived" but not all "young" sources, it will be of great interest to investigate whether CSO 2s show the same strong cosmological evolution as do both high-luminosity extended steep spectrum sources and compact flat spectrum sources (Peacock & Gull 1981), but this is beyond the scope of the present paper.

5. The Size Distribution of CSOs

Our third independent test of the hypothesis that CSO 2s form a distinct class of jetted AGN is based on the size

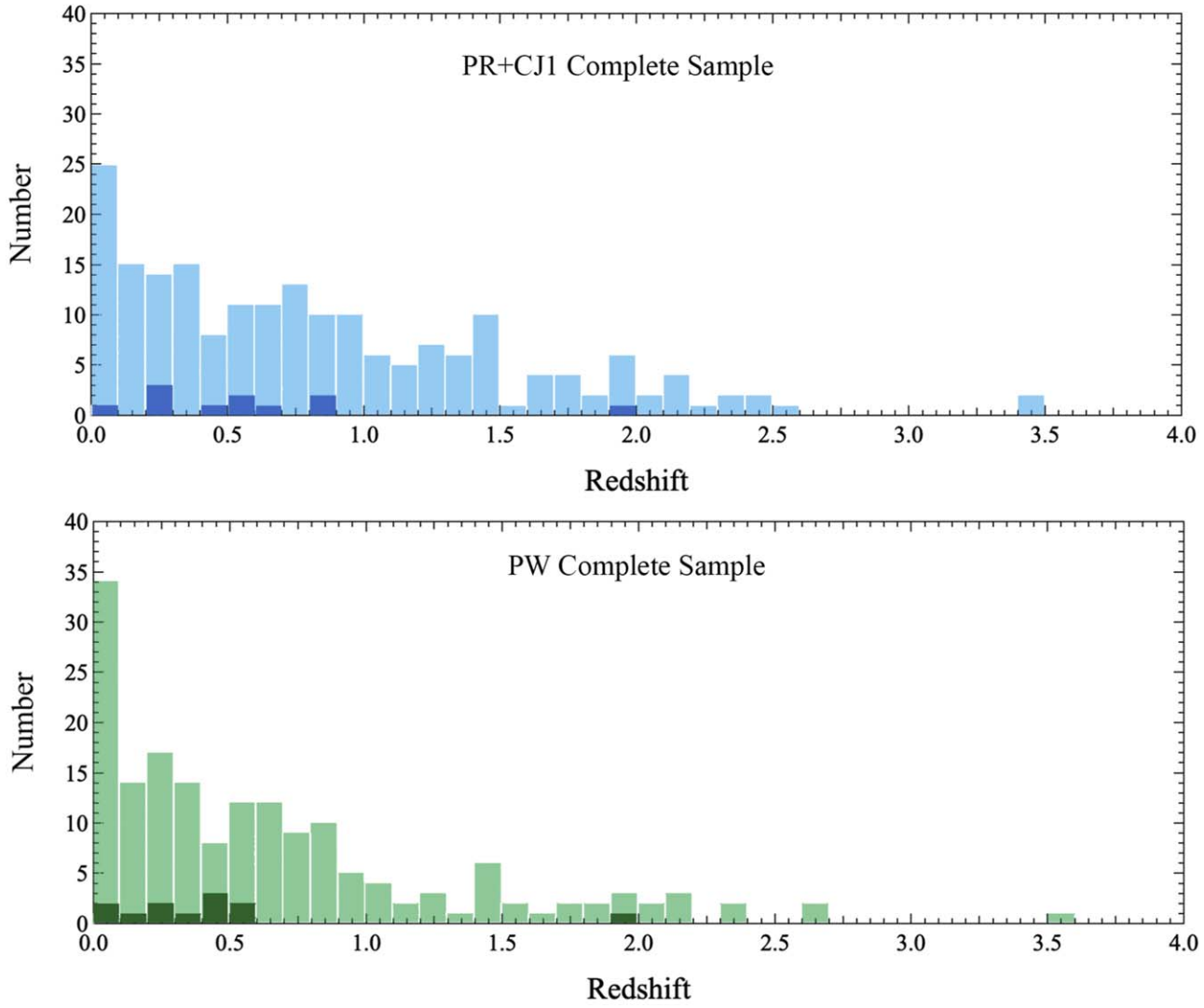

Figure 2. The redshift distributions for the PR+CJ1 complete sample (top panel) and the PW complete sample (bottom panel). The light shaded distributions show the complete samples. The dark shaded regions show the CSO 2s. Note that these distributions are not stacked vertically, so the values on the ordinate represent the total numbers of sources and the numbers of CSO 2s in each sample. The cumulative distributions and K-S statistics are shown in Figures 3(a) and (b).

Table 4
Two-sample K-S Tests of CSO Redshifts as a Distinct Population

Test Number	Complete Sample	Sky Area	Flux Density Limit	Frequency (GHz)	K-S Statistic	p-value	Significance
1	PR+CJ1	$\delta > 35°$, $\lvert b\rvert > 10°$	0.7 Jy	5	0.34	1.3×10^{-1}	1.1σ
2	PW	$\delta > 10°$, $\lvert b\rvert > 10°$	1.5 Jy	2.7	0.41	3.1×10^{-2}	1.9σ
3	PWS	$10° < \delta < 35°$, $\lvert b\rvert > 10°$	1.3 Jy	5	0.52	1.2×10^{-1}	1.3σ
4	PR+CJ1+PWS	⋯	⋯	5	⋯	1.6×10^{-2}	2.1σ

Note. Tests #1 and #3 are independent due to their the different sky areas. We can therefore, legitimately, multiply their p-values, which we do in Test #4. While the results of this redshift test do not rise to the 3σ level, and so cannot be considered to be compelling in and of themselves, they do strongly suggest a difference between most CSO 2s and the rest of the jetted AGN population, and are therefore supportive of the other tests we present.

distribution of CSO 2s. This test is more complex and more subject to selection effects than the tests of the previous two sections. Selection effects are particularly strong when it comes to consideration of the observed distribution of CSO sizes, so we discuss first the effectiveness of our approach in dealing with these selection effects, in order to give the reader some confidence in the statistical robustness of our results.

5.1. The Efficacy of Complete Samples in Dealing with the CSO Size Distribution Selection Effects

The distribution of the physical sizes of the 54 bona fide CSO 2s, out of our sample of 79, for which we have spectroscopic redshifts is shown in Figure 4(a). It shows a strong cutoff well below 1 kpc. However, one has to bear in mind that this sample of 54 bona fide CSO 2s is a heterogeneous sample gleaned from the literature, and is subject to selection effects. We therefore

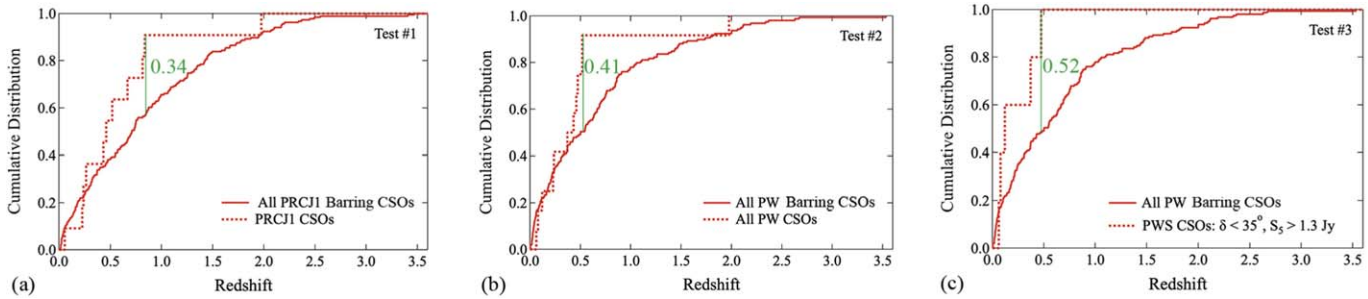

Figure 3. K-S Tests on the redshift distributions of the bona fide CSO 2s in the PR+CJ1, PW, and PWS samples. (a), (b), and (c): comparison of the CSO cumulative redshift distributions vs. the non-CSO 2s in the complete PR+CJ1, PW, and PWS samples, respectively. The green bars indicate the maximum differences in the cumulative distributions, corresponding to the values of the K-S statistic given by the numbers in green. The corresponding *p*-values are listed in Table 4.

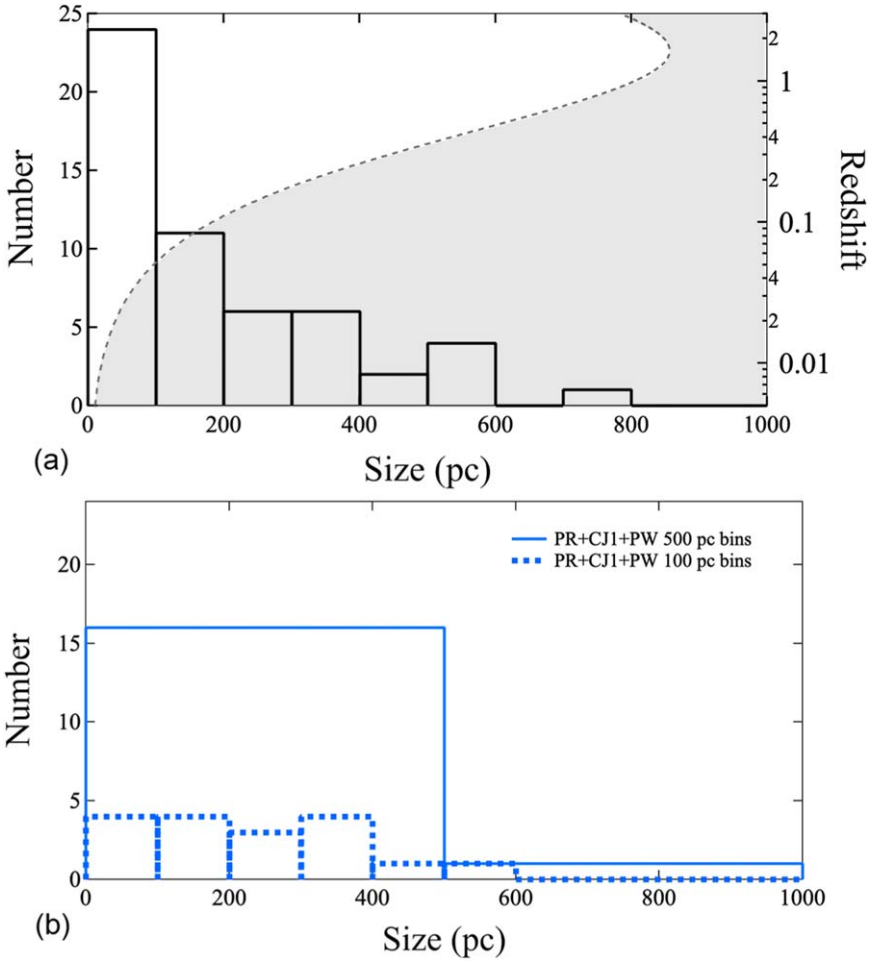

Figure 4. The distributions in size of the bona fide CSOs over the whole CSO size range, from 0 pc to 1 kpc. (a) The heavy black boxes show the histogram of the sample of 54 bona fide CSOs for which there are spectroscopic redshifts, with the numbers given on the left axis. The dashed curve, marking the border of the shaded region, shows the physical size corresponding to 100 mas at the redshift indicated on the right-hand axis. For typical VLBI observations at 5 GHz and above, CSOs in the grayed region to the right of this curve would be hard to observe, so there is a strong selection effect that might account for the drop in the number of bona fide CSOs with physical size. (b) The 17 bona fide CSO 2s with spectroscopic redshifts in the complete flux density–limited PR+CJ1+PW sample. Dotted curves show the data binned into 100 pc bins, while solid curves show the data binned into 500 pc bins. The K-S and binomial tests both show that this distribution differs from a uniform distribution at the *p*-value $\sim 1.7 \times 10^{-4}$ (3.6σ) level. While the observed uneven distribution could just be a result of small statistics, it would be foolish to ignore it, especially in light of the corroborating evidence from both the numbers and the redshift distributions. Nature often surprises us.

have to consider carefully whether these selection effects can be eliminated in complete subsamples of our 54 bona fide CSO 2s.

5.1.1. The ∼100 mas Selection Effect

The first selection effect we consider comes about because the largest angular size that is measured in most centimeter-wavelength VLBI maps is ∼100 mas. In Figure 4(a) we show the upper size cutoff this would impose as a function of redshift. Only CSOs to the left of this curve have an angular sizes less than 100 mas at the corresponding redshift. Clearly this could well impose a strong selection effect on the observed size distribution of CSOs.

On the face of it, it might appear that this selection effect alone is so strong that the true size distribution of CSOs is impossible to determine from these data. Fortunately this is not the case because

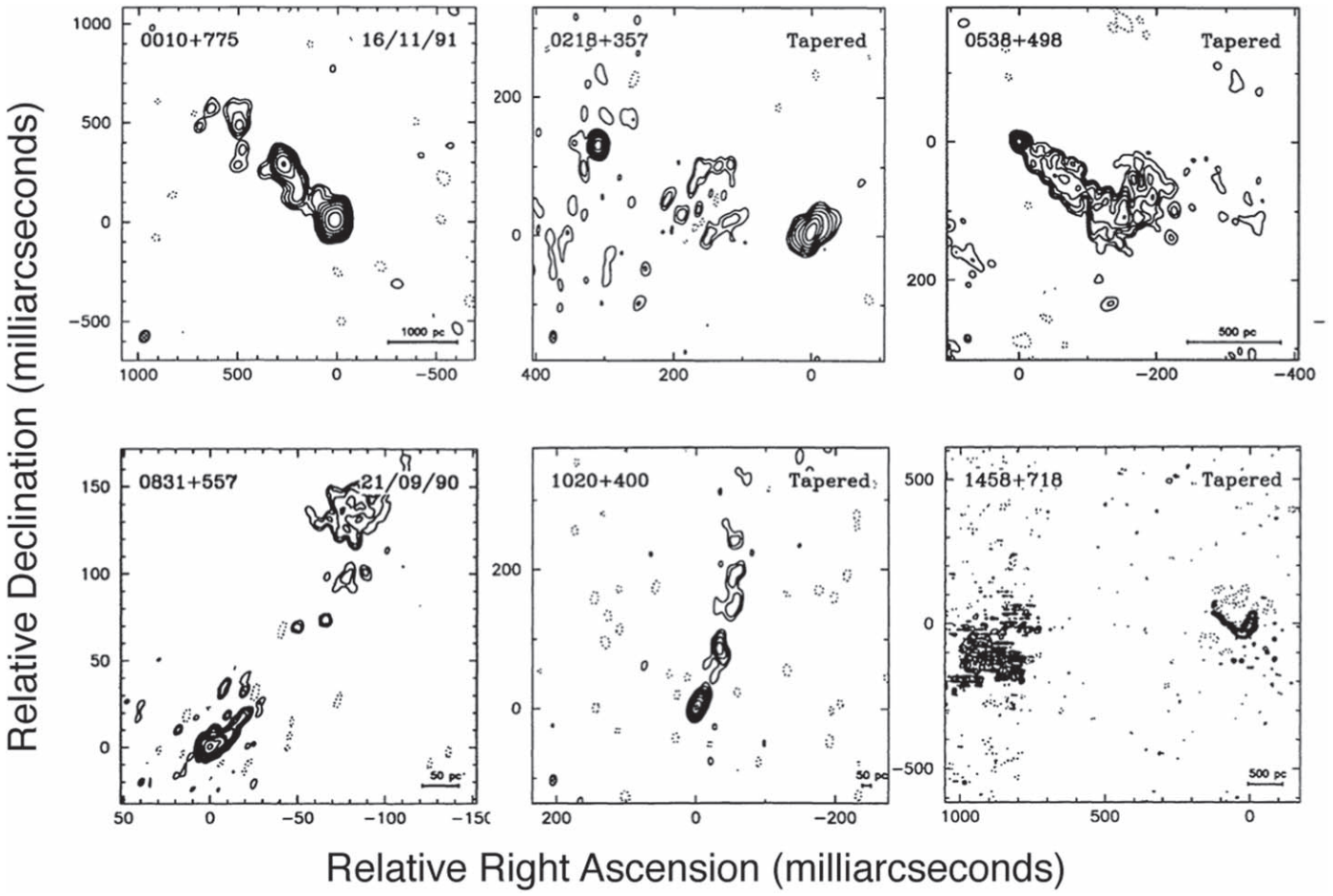

Figure 5. Demonstration that the complete samples studied in this paper are not restricted by the usual ∼100 mas field sizes typical of most VLBI observations at 5 GHz. Shown here are 1.7 GHz VLBI maps of six large angular scale compact AGN from the CJ1 complete sample survey (Polatidis et al. 1995), all of which have sizes ≫100 mas. Note that the structure of 1458+718 (J1459+7140, 3C 309.1) extends over 1″—i.e., the map is 10 times larger than the typical field of view of VLBI maps at 5 GHz or higher frequencies.

(i) one can observe complete samples in which one knows the sizes of all the objects in the sample, and (ii) if some objects are too large for VLBI mapping at centimeter wavelengths they can be observed at longer wavelengths, where the ∼100 mas limit does not apply. We have availed ourselves fully of both of these strategies by (i) using complete samples, and (ii) in addition to the observations of compact objects in the PR+CJ1 complete samples at 5 GHz (Pearson & Readhead 1988; Xu et al. 1995), all of these objects were observed at 1.66 GHz (Polatidis et al. 1995; Xu et al. 1995). In Figure 5 we show examples of six AGN from the CJ1 complete sample with sizes far exceeding the 100 mas angular size limitation of regular VLBI at 5 GHz and above. As can be seen here, even objects as large as 1″ were mapped in this survey. This is one of two reasons we can be confident that we have not missed any large CSOs in these complete samples. The other reason is that the large —by which we mean (≳1″)—and small-scale radio structures of *all* of these objects are known. In Table A1 in the Appendix we list references which present the relevant maps of all 281 objects in the PR+CJ1+PW samples.

5.1.2. Spectral Shape Selection Effect

Many CSOs are peaked spectrum (PS) sources.[12] Thus in a sample of CSOs selected at a single frequency, we will clearly include all of the sources that peak at that frequency down to the flux density limit. However, for sources that peak at frequencies significantly higher or lower than the selection frequency, the sample will exclude an increasing number of the CSOs as the separation between the peak frequency and the selection frequency increases. In this study, we therefore consider not only the PR+CJ1 and PW samples, selected at 5 and 2.7 GHz, but we also consider the GLEAM sample, observed using 20 simultaneous flux density measurements spanning frequencies between 72 and 231 MHz, the 3CRR sample selected at 178 MHz, and the Jodrell Bank 966 MHz sample.

The situation is illustrated in Figure 6. The blue points show the observed radio spectrum of OQ 208 (J1407+2827; Stanghellini et al. 1997), which has one of the narrowest, most sharply peaked, spectra among the bona fide CSO 2s. The gray points illustrate an object with the same spectral shape as OQ 208, but with the maximum shifted from 5 GHz down to 1 GHz, and the peak flux density shifted down to 1.3 Jy. This is the point where the object would drop below the GLEAM 1 Jy limit (Callingham et al. 2017), and the CJ1 700 mJy limit. Because of the drop-off in flux density, relative to the peak, at both higher and lower frequencies, such an object would not be included in the PW, PR, CJ1, or GLEAM samples. Objects of this type with peak flux densities greater than 1.3 Jy would, however, be included in the GLEAM and CJ1 samples, whose

[12] In this paper we follow the lead of OS21 in their comprehensive review, and refer to GPS and MHz peaked specrrum sources as PS sources.

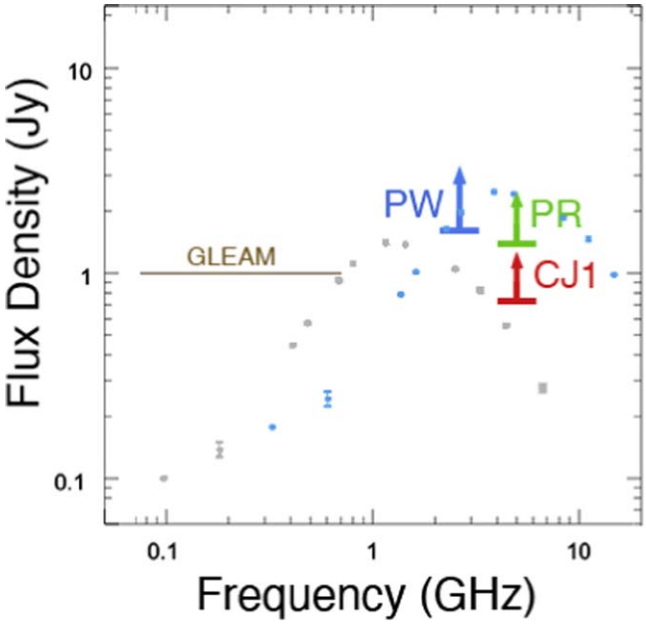

Figure 6. CSO 2s that might be missed in the PR, CJ1, and PW complete samples due to spectral effects. The blue, green, and red arrows indicate the selection frequency and limiting flux densities of the PW, PR, and CJ1 samples, respectively. The horizontal brown line indicates the flux density limit of the GLEAM sample. The blue and gray points show the observed spectrum of OQ 208 (Stanghellini et al. 1997), and a shifted spectrum of OQ 208, respectively (see the text).

limiting flux densities are indicated by the horizontal brown line in Figure 6, and the red horizontal bar, respectively. We therefore consider next what is known about the population of objects that peak at frequencies $\lesssim$1 GHz.

The GLEAM survey covers 72–700 MHz, and is concentrated in the Southern Hemisphere, and so overlaps only part of the sky area covered by the PR+CJ1+PW sample, but it complements the higher-frequency VLBI surveys that have studied complete samples because of its lower frequency. 505 of the 11,400 sources in the complete 1 Jy GLEAM sample ((4.4 ± 0.2)%) are PS objects (Callingham et al. 2017), with peak flux densities above 1 Jy in the 72–700 MHz range, and so must also be compact (Readhead et al. 2021). Similarly, in a LOFAR study of northern radio sources at 150 MHz, Slob et al. (2022) found 373 PS sources and concluded that ∼2.5% of sources in complete samples around 150 MHz are PS sources. We note the similarity in the fractions of PS sources identified in the LOFAR (150 MHz), GLEAM (72–700 MHz), and the fraction of PW+CJ1+PW (2.7 and 5 GHz) CSO 2s samples, which are ∼2.5%, ∼4.4%, and ∼6.8%, respectively. It is possible that a significant fraction of the PS population in both the LOFAR and GLEAM surveys are CSO 2s, and thus that there is a significant population of CSO 2s extending to below 100 MHz. In this case we could well be missing CSO 2s that could fall into in the 500 pc–1 kpc size range. In Figure 7 we show the sizes of the PR+CJ1+PW CSO 2s plotted against peak frequency. It is interesting to note that almost half of these objects have peak frequencies in the range covered by the GLEAM survey, even though they were selected at 2.7 GHz and/or 5 GHz. It is also interesting to note that, apart from the small fraction (<25%) that has peak frequencies above 3 GHz, there is no clear dependence of size on frequency.

5.2. A Spectral Shape Lacuna

As we have seen in the previous sections, we are only considering the 17 bona fide CSO 2s in the PR+CJ2+PW complete sample with known spectroscopic redshifts, and there are only two bona fide CSOs in these complete samples without a spectroscopic redshift. The PR+CJ2+PW complete sample, including M82, consists of the 282 sources listed in Table A1. In 5.1.2 we discussed a spectral shape selection effect that can be affecting this sample. The GLEAM survey detected 11,400 sources with flux densities greater than 1 Jy between 70 and 700 MHz. Of these 505 are PS sources. In order to double the numbers of CSO 2s, and hence potentially to have a strong effect on any statistical tests of the size distribution of CSO 2s, there would need to be ≈17 bona fide CSO 2s in the GLEAM sample. Thus only a small fraction ∼3% (17/505) of the PS sources in the GLEAM would need to be CSO 2s in order potentially to have a significant impact on the statistics. So this is a lacuna that has to be addressed in any size tests.

In the next three subsections we advance two independent arguments to address this lacuna and we suggest a test that could fill the lacuna, but which requires more observations and is therefore beyond the scope of the present paper.

5.2.1. The Range of Peak Frequencies in Our Sample

In Figure 6 of Paper I we have plotted the range of peak frequencies observed, and it can be seen that the peak frequencies range from below 80 MHz to ∼10 GHz. The same is true of the objects in our combined PR+CJ1+PW sample—the lowest peak is at 70 MHz and the highest peak is at 6.4 GHz, and the distribution of the peaks is roughly uniform between these extremes.

Thus the selection procedure of the complete PR+CJ1+PW sample and our bona fide CSO identification method do not appear to have created a bias against CSO 2s peaking anywhere within this range. However, while the (rarer) flat spectrum CSO 2s will not suffer from the spectral selection biases described earlier, some PS CSO 2s could be excluded from the sample for certain redshift ranges. This could, therefore, influence the size distribution of the observed CSO 2s in the PR+CJ1+PW samples, particularly if CSO intrinsic size is related to peak frequency and/or luminosity.

In the next two subsections we give an argument that shows that spectral shape selection effects are unlikely to have biased the size distribution of the CSO 2s in the PR+CJ1+PW sample.

5.2.2. The 3CRR and PW CSS Double Sample

In addition to our complete samples of CSO 2s, described in the previous sections, there is one other relevant sample of CSO 2s and MSOs that has been studied extensively by the Bologna group (BG), the key results of which are given in a series of papers (Fanti et al. 1985, 1990; Spencer et al. 1991; Dallacasa et al. 1995; Fanti et al. 1995; Dallacasa et al. 2013, 2021). The BG identified 32 double-lobed CSS objects, given in Table 1 of Fanti et al. (1995), in their sample drawn from the 3CRR (Laing et al. 1983) and the PW samples. They subsequently added one double-lobed source (1819+396 = 4C +39.56) that they had previously missed (Dallacasa et al. 2021), bringing the total of double-lobed CSS sources in the BG sample to 33. Given that these are CSS objects, they excluded flat spectrum objects with $\alpha > -0.5$.

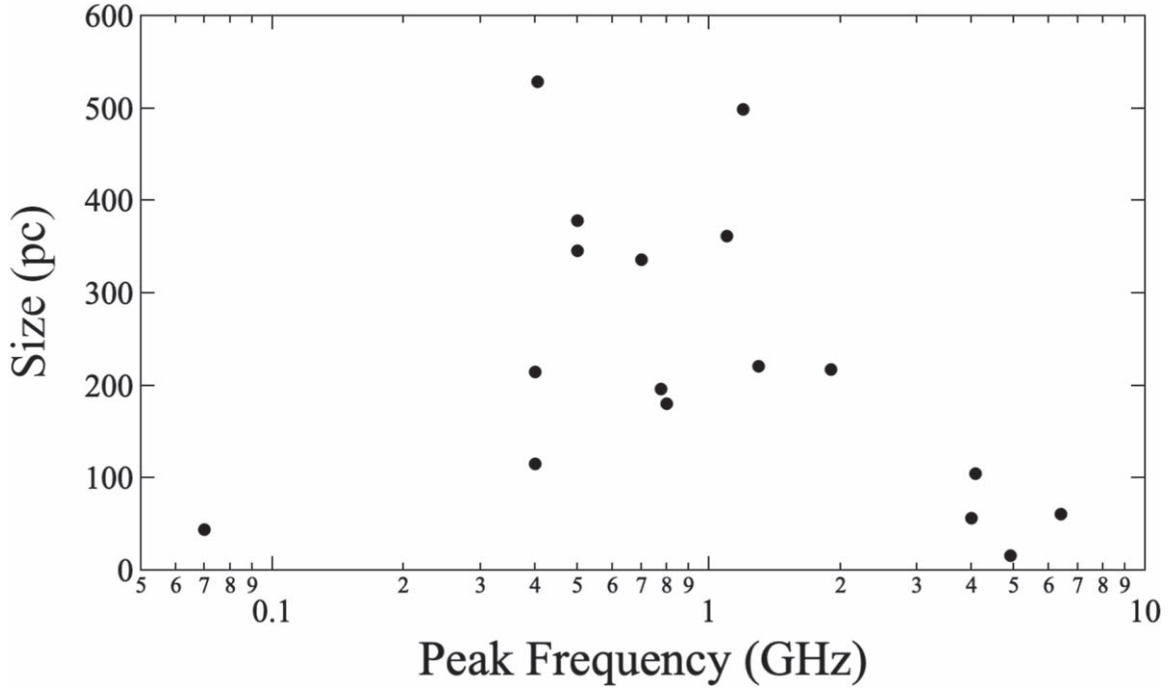

Figure 7. The relationship between size and peak frequency for the CSO 2s in the PR+CJ1+PW complete sample.

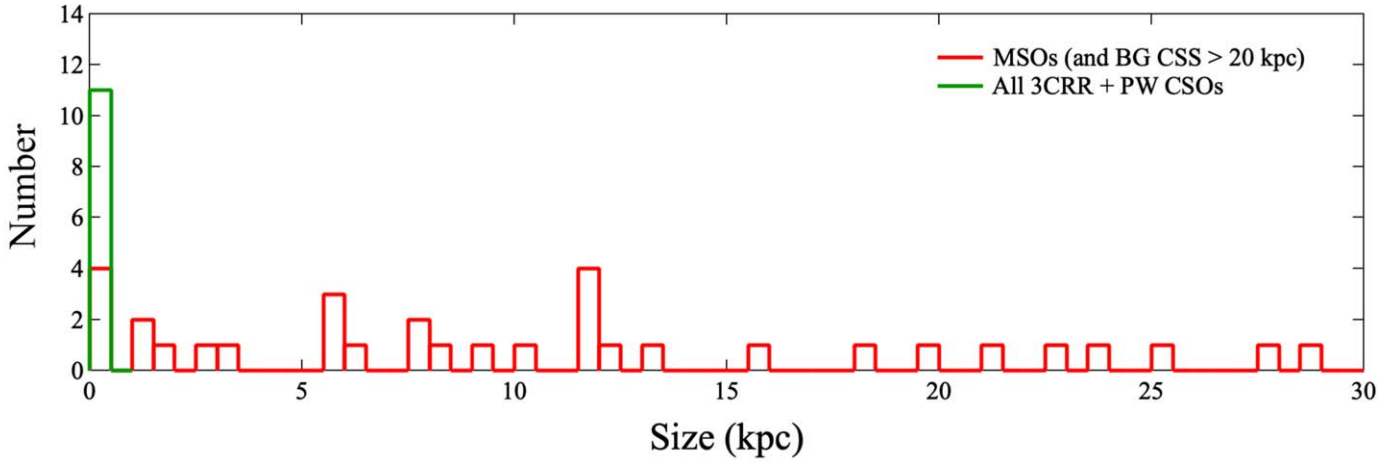

Figure 8. The distributions of the bona fide CSO 2s and MSOs as a function of projected physical size in the BG sample. The red distribution shows the BG CSO 2s +MSOs+CSS > 20 kpc objects. The green distribution shows the BG+PW CSO 2s.

This spectral filter against flat spectrum sources ($\alpha > -0.5$), as applied to the 3CRR sample, which has a limiting flux density of 10 Jy at 178 MHz, excludes sources brighter than 2.57 Jy at 2.7 GHz. Since these are greater than the flux density limit of the PW complete sample (1.5 Jy at 2.7 GHz), any such object can be included in the BG study by adding the flat spectrum PW CSO 2s to the steep spectrum CSO 2s detected by the BG, in order to get the total of both flat and steep spectrum compact doubles, including CSO 2s, in the 3CRR and PW samples (note that there are no flat spectrum doubles of size greater than 1 kpc in PW). There are four BG CSO 2s in our sample of 79 bona fide CSO 2s listed in Paper I. All four of these BG CSOs are already in our complete sample of CSOs in the PR+CJ1+PW complete samples.

We therefore compensate for the spectral index limit in BG sample by adding the flat spectrum PW bona fide CSO 2s that were excluded from the BG sample by the spectral index cutoff at $\alpha = -0.5$ to the BG sample of CSO 2s, thereby making this into a complete sample of 3CRR+PW compact double sources, and bringing the total including the PW flat spectrum CSO 2s to 40. In order to apply the same largest angular size filter as that used in Paper I, we have remeasured the largest angular sizes of the 33 BG CSS double sources at the lowest frequency at which high-quality maps are available in the BG group's publications listed above. The results are shown in Figure 8, together with the seven flat spectrum PW bona fide CSO 2s that we have added.

We find that 27 of the 33 objects in the BG sample fit the CSO+MSO criteria, with four of the objects being bona fide CSO 2s and the remaining 23 objects being MSOs. The six remaining objects all have largest projected physical sizes greater than 20 kpc, based on our measured largest angular sizes. When we add the flat spectrum objects from the PW sample, the number of CSO 2s increases from four to 11, as shown in Figure 8.

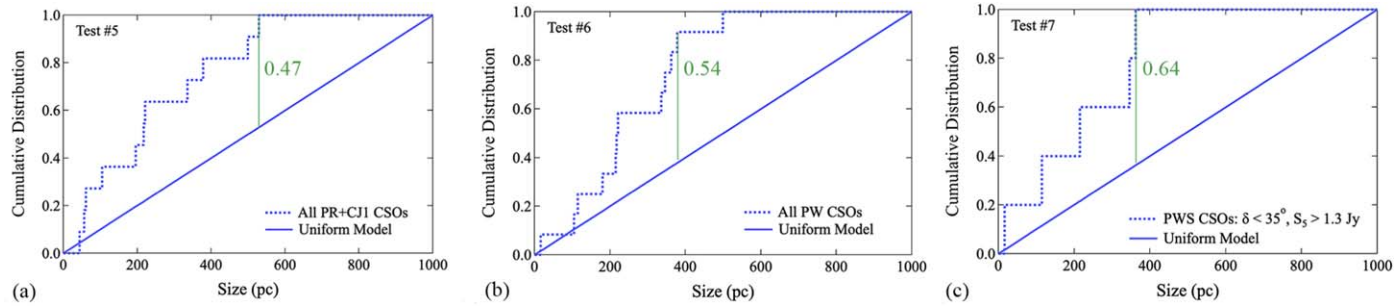

Figure 9. K-S Tests on the size distributions of the bona fide CSO 2s in the PR+CJ1 and PW samples. (a), (b) and (c): comparison of the CSO 2 cumulative size distributions vs. the uniform model for the PR+CJ1, PW, and PWS samples, respectively. The green bars indicate the maximum differences in the cumulative distributions, corresponding to the values of the K-S statistic given by the numbers in green. The corresponding *p*-values are listed in Table 5.

Table 5
One-sample K-S Tests against a Uniform Distribution of the CSO 2 Sizes

Test Number	Complete Sample	Sky Area	Flux Density Limit	Frequency (GHz)	K-S Statistic	*p*-value	Significance
5	PR+CJ1	$\delta > 35°$, $\lvert b\rvert > 10°$	0.7 Jy	5	0.47	9.3×10^{-3}	2.4σ
6	PW	$\delta > 10°$, $\lvert b\rvert > 10°$	1.5 Jy	2.7	0.54	8.7×10^{-4}	3.1σ
7	PWS	$10° < \delta < 35°$, $\lvert b\rvert > 10°$	1.3 Jy	5	0.64	1.7×10^{-2}	2.1σ
8	PR+CJ1+PWS	⋯	⋯	5	⋯	1.6×10^{-4}	3.6σ

Note. Tests of the observed CSO 2 size distribution compared to a uniform size distribution. The PWS sample is the effectively complete subsample of the PW sample having $10° < \delta < 35°$, $\lvert b\rvert > 10°$ and $S_{5\ \mathrm{GHz}} \geqslant 1.3$ Jy (see the text).

The four CSO 2s in the BG CSS sample all have sizes between 300 pc and 500 pc. These PS CSO 2s have spectral turnovers that are almost certainly due to synchrotron self-absorption as is shown in the paper by Scott & Readhead (1977), who showed that the equipartition angular size $\psi_{\mathrm{eq}} \propto S^{\frac{8}{17}} \nu^{-\frac{35+2\alpha}{34}} (1+z)^{\frac{15-2\alpha}{34}}$. Thus fainter objects that show spectral peaks at higher frequencies will be smaller than the four CSS CSO objects in the BG sample. It therefore is unlikely that there will be a significant number of CSS CSO 2s with sizes in the 500 pc to 1 kpc range. We return to this point in Section 5.3.

5.2.3. The Jodrell Bank 966 MHz Sample

Since the 3CRR sample is complete down to 10 Jy at 178 MHz (Laing et al. 1983), for comparison with the other samples in this study it would be helpful to have a low-frequency sample complete down to ∼1 Jy. Fortunately, such a sample exists for which the radio structures of over 98% of the objects are known.

Referring back to Figure 6 and the objects in the lacuna illustrated by the gray spectrum, we can define a complete sample drawn from the Jodrell Bank 966 MHz survey (Cohen et al. 1977), which produced a radio catalog and measured arcsecond-level positions for the majority of its sources. We have selected a subsample consisting of 169 of the strongest sources ($S_{0.966\ \mathrm{GHz}} > 1.5$ Jy) from Cohen et al. (1977). This subsample is unbiased, and while the full survey is not strictly complete due to confusion issues, these apply only at low flux density levels, and thus the subsample that we have selected is not affected by confusion. We will refer to this unbiased subsample of 169 objects as the "JBS" sample.

We classified 74 of the JBS sample in the filtering process we carried out in selecting our bona fide CSO 2s described in Paper I. We identified six of them as bona fide CSO 2s.

We have extracted VLA Sky Survey (VLASS; Lacy et al 2020) cutout images of all 169 JBS objects using the CIRADA cutout server,[13] and we found only 17 of them to be unresolved, with largest angular size $<3''$, and hence possible CSO 2s. Of these 17 compact objects, two are MOJAVE "core–jet" objects, and one is a $2''$ double. Thus there are 14 possible CSO 2s in the 966 MHz JBS sample in addition to the six bona fide CSO 2s we have already identified. We are engaged in obtaining VLBI observations of these 14 objects.

5.3. Statistical Analysis of CSO Sizes in the Complete Samples

As we have seen, all of the bona fide CSOs in the complete PR, CJ1, and PW samples are CSO 2s—i.e., as discussed in Paper I, they are edge-brightened, high-luminosity objects. This is a selection effect resulting from the flux density limits in the complete samples. The size distribution of the CSO 2s in the PR+CJ1+PW complete sample is shown in Figure 4(b), binned into 100 pc and 500 pc intervals.

Using the CSO 2 size distributions in the PR+CJ1 and PW complete samples, we have carried out two sets of statistical tests of the hypothesis that CSO 2s are uniformly distributed in size between 0 and 1000 pc, as would be expected on the hypothesis that the speed of advance is constant: (i) a set of K-S one-sample tests, which yield the cumulative distributions shown in Figures 9(a), (b) and (c) and the *p*-values shown in Tests #5–#8 in Table 5; and (ii) binomial tests in which we divided the CSO 2s into two size bins, from 0 to 500 pc, and from 500 to 1000 pc, which yield the results shown in Table 6.

We consider first the K-S tests shown in Table 5. We see there that the uniform hypothesis is rejected by the PR+CJ1 CSO sample at the 9.3×10^{-3} probability level, and by the PW CSO sample at the 8.7×10^{-4} probability level. The independent, effectively complete, PW CSO sample below a decl. of 35° (Test #7) rejects the uniform hypothesis at the 1.7×10^{-2} level.

[13] http://cutouts.cirada.ca

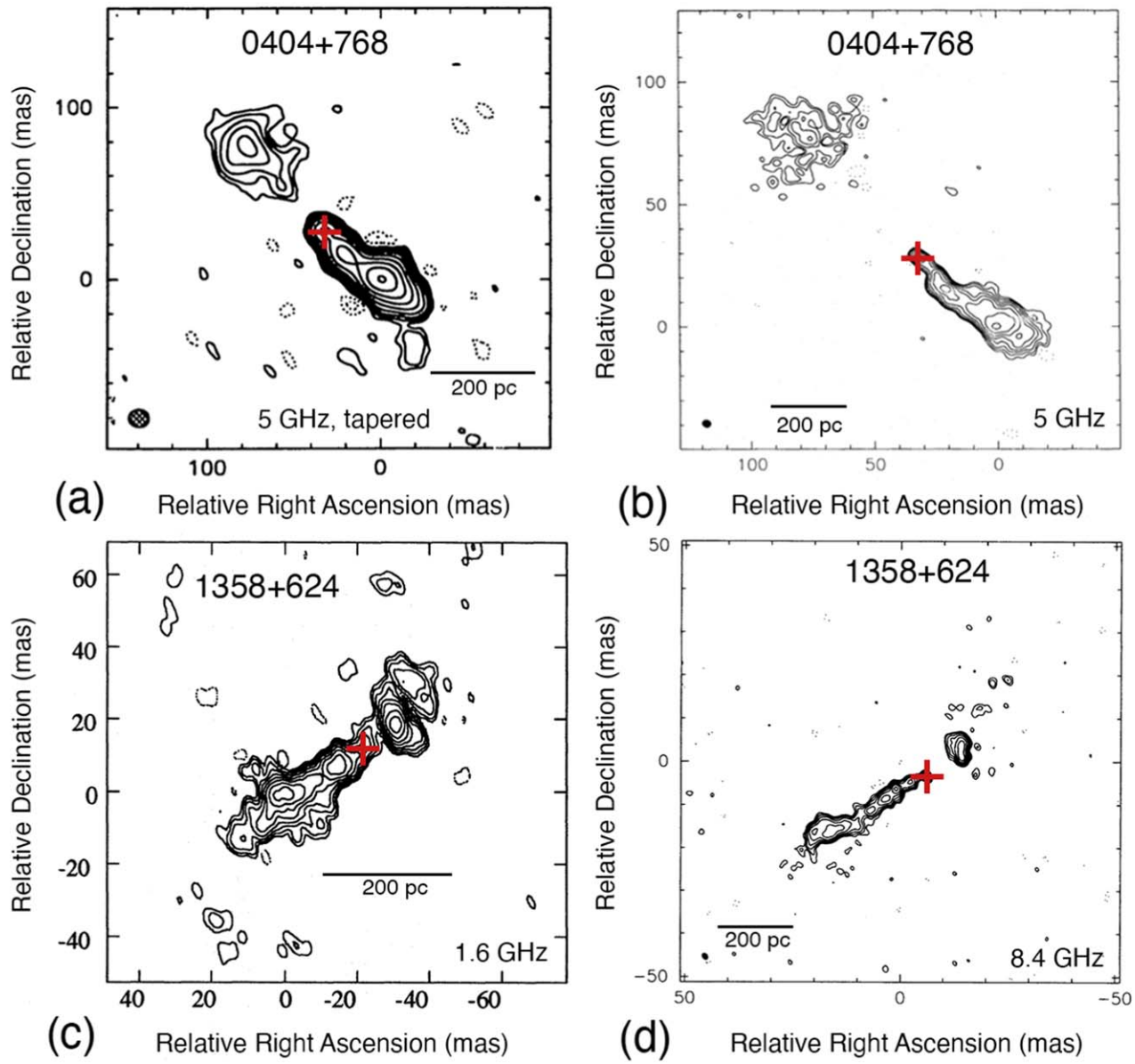

Figure 10. Example of an MSO and a CSO with similar morphologies. (a) The MSO 0404+768 (J0410+7656) is from (a) Xu et al. (1995) and (b) from Taylor et al. (1996), which these authors had classified as a CSO. The CSO 1358+624 (J1400+6210) from (c) Dallacasa et al. (1995) and (d) Taylor et al. (1996). Some CSO 2s must evolve into MSOs and 1358+624 may be just such a case. The red cross marks the location of the core in each map.

Tests #5 and #7 are independent—note the different sky areas—and at the same observing frequency. We can therefore, legitimately, multiply their p-values. This gives Test #8, which rejects the uniform size distribution hypothesis at the p-value 1.6×10^{-4}, or 3.6σ significance level.

The results of the binomial tests, shown in Table 6, show that by similarly combining the PR+CJ1 CSO sample (Test #9) with the independent PWS sample (Test #10), as shown in Test #11, the uniform hypothesis is rejected at the 1.7×10^{-4} (3.6σ) level.

In our view, these tests on complete samples constitute compelling evidence that the size distribution of CSO 2s cuts off sharply at ≈500 pc, which is significantly below the 1 kpc size limit imposed by the defining criteria of CSOs. As described in Section 5.2.3, the existence of this sharp cutoff can be tested, for example, with MERLIN and VLBI observations of the 14 potential CSO 2s in the complete JBS sample.

Clearly *some* CSO 2s must grow to larger sizes in order to produce MSOs, FR Is, and FR IIs. An example of a CSO and MSO with remarkably similar morphologies is shown in Figure 10, which illustrates this point, especially since 0404+768 (J0410+7656) was originally classified as a CSO, but fails the size cutoff (by ∼20%). It is clear that the majority of CSO 2s do not grow much above 500 pc in projected size.

6. Results and Tests from This Paper

The results and tests that have come out of this study are listed below.

Table 6
Binomial Tests of the Significance Levels of the CSO Size Distributions in the Complete Samples

Test Number	Complete Sample	Sky Area	α Limit	N 0–500 pc	N 500 pc–1 kpc	p-value	Significance
9	PR+CJ1	$\delta > 35°$, $\lvert b\rvert > 10°$	⋯	11	1	5.4×10^{-3}	2.6σ
10	PWS	$\delta < 35°$, $\lvert b\rvert > 10°$	⋯	6	0	3.1×10^{-2}	1.9σ
11	PR+CJ1+PWS	⋯	⋯	⋯	⋯	1.7×10^{-4}	3.6σ

Note. The PR+CJ1 and PWS ($\delta < 35°$, $S_5 > 1.3$ Jy) samples are independent, so we have multiplied their p-values in Test #11 (see the text).

6.1. Results

The number fraction, redshift, and size statistics discussed in the previous three sections and presented in Tables 4 to 6 demonstrate that (i) most CSO 2s are drawn from a population of jetted AGN that is distinct from other jetted AGN, and (ii) the size distribution of CSO 2s cuts off sharply at ≈500 pc, a finding that is verifiable (see Section 5.2.3).

These are significant findings. They show that there has to be something fundamentally different between CSO 2s and the larger sources. While both must be driven by the same type of central engine, since both are producing high-luminosity relativistic jets, there must be some fundamental difference between them to produce two such different outcomes—one with a size cutoff around 500 pc and the other with a size cutoff ∼200× larger.

One might think, for example, that the cutoff could be explained simply by random episodic fueling. But how would random episodic fueling produce a sharp cutoff? Random episodic fueling would produce a uniform distribution. There has to be another explanation for the cutoff, such as, for example, an upper limit on the size of the fuel packages, a change in the jet environment that leads the jets to fade beyond a certain distance from the central engine, or a mechanism associated with the accretion disk that limits the energy of the jet.

6.2. Tests

The major tests resulting from this paper are the following:

1. We will follow up the JBS sample with MERLIN and VLBA observations in order to test the sharp cutoff in size we have seen in the PR+CJ1+PW complete sample.
2. We have undertaken a program to increase the number of CSO 2s in complete samples by a factor of at least three, to ∼50, by carrying out a VLBI survey of 332 steep spectrum sources that complement the VIPS flat spectrum survey, thus converting VIPS into a complete sample. This will further test the cutoff in CSO 2 size distribution.
3. Morpholocial studies of the PS objects identified in the LOFAR and GLEAM surveys would be well worth doing.

7. Discussion

Although the selection effects inherent in our literature search for CSOs are significant, we have shown that, with careful use of complete samples, and using the 17 CSO 2s in the complete PR, CJ1, and PW samples for which we have spectroscopic redshifts, it is possible to carry out a series of rigorous statistical tests that provide what we regard as compelling evidence that the vast majority of CSO 2s constitute a population of jetted AGN that is distinct from, and therefore requires a separate origin to, the larger classes of jetted AGN, such as CSS sources, MSOs, and FR I and FR II objects.

The physical size cutoff is clearly telling us something important about this class of jetted AGN. The scenario that produces almost all CSO 2s must be different in some important way from that which produces the larger symmetric radio sources. We return to this discussion of the origins of CSO 2s in Paper III.

It should be clear, therefore, that, (i) because the observed emission regions in these objects are not significantly relativistically boosted toward the observer, thereby making it possible to determine their detailed physical properties, and (ii) most CSO 2s belong to a distinct class of jetted AGN, these CSO 2s provide a unique time domain plus structural window on the central engines of jetted AGN and the SMBHs that drive them.

Acknowledgments

We thank John Peacock for useful discussions. We thank the reviewer of this paper for many helpful suggestions that have clarified several important aspects of this work. We are grateful for the use of the CATS database of Verkhodanov et al. (2005), of the Special Astrophysical Observatory. This research has made use of NASA's Astrophysics Data System Bibliographic Services. This research has made use of the NASA/IPAC Extragalactic Database (NED) which is operated by the Jet Propulsion Laboratory, California Institute of Technology, under contract with the National Aeronautics and Space Administration. This research has made use of data from the OVRO 40-m monitoring program (Richards et al. 2011), supported by private funding from the California Insitute of Technology and the Max Planck Institute for Radio Astronomy, and by NASA grants NNX08AW31G, NNX11A043G, and NNX14AQ89G and NSF grants AST-0808050, AST-1109911, and AST-1835400. This research has made use of data from the MOJAVE database that is maintained by the MOJAVE team (Lister et al. 2018). The MOJAVE program is supported by NASA-*Fermi* grant 80NSSC19K1579. This research has made use of the CIRADA cutout service at http://cutouts.cirada.ca, operated by the Canadian Initiative for Radio Astronomy Data Analysis (CIRADA). CIRADA is funded by a grant from the Canada Foundation for Innovation 2017 Innovation Fund (Project 35999), as well as by the Provinces of Ontario, British Columbia, Alberta, Manitoba, and Quebec, in collaboration with the National Research Council of Canada, the US National Radio Astronomy Observatory and Australia's Commonwealth Scientific and Industrial Research Organisation. S.K. and K.T. acknowledge support from the European Research Council (ERC) under the European Unions Horizon 2020 research and innovation program under grant agreement No. 771282. K.T. acknowledges support from the

Foundation of Research and Technology—Hellas Synergy Grants Program through project POLAR, jointly implemented by the Institute of Astrophysics and the Institute of Computer Science. A.S. was supported by the NASA Contract NAS8-03060 to the Chandra X-ray Center.

This paper depended on a very large amount of VLBI data, almost all of which was taken with the Very Long Baseline Array. The National Radio Astronomy Observatory is a facility of the National Science Foundation operated under cooperative agreement by Associated Universities, Inc.

Appendix

In Table A1 we show the relevant properties and references for the 282 objects in the PR, CJ1, and PW complete samples.

Table A1
Structure Types and Literature References for the Combined PR, CJ1, and PW[b] Samples

B1950 Name	J2000 Name	Alias	PR	CJ1	PW	Type	Optical ID[c]	Large-scale Structure	Small-scale Structure
(1)	(2)	(3)	(4)	(5)	(6)	(7)	(8)	(9)	(10)
0010+775	J0013+7748	S5 0010+77		Y		CT, CSS	G		41 ,42
0010+405	J0013+4051	4C +40.01		Y		CT, CFS	G		41, 42
0013+790	J0016+7916	3C 6.1		Y	Y	FR II	G	3, 9, 62	
0016+731	J0019+7327	S5 0016+73	Y		Y	U, CFS	Q	9	31
0022+390	J0025+3919	S4 0022+39		Y		CT, CFS	Q		41, 42
0026+34	J0029+3456	B2 0026+34			Y	CSO	G		58, 67
0038+32	J0040+3310	3C 19			Y	FR II	G	8, 9, 62	
0040+517	J0043+5203	3C 20	Y		Y	FR II	G	8, 9, 64	
0048+509	J0050+5112	3C 22.0		Y		FR II	G	8	
0102+480	J0105+4819			Y		CT, CFS			41, 42
0104+32	J0107+3224	3C 31			Y[b]	FR I	G	8,9	
0106+13	J0108+1320	3C 33			Y[b]	FR II	G	9,34	
…	…	…	…	…	…	…	…	…	…
2251+15	J2253+1608	3C 454.3			Y[b]	U, CFS	Q	9,58	
2252+12	J2255+1313	3C 455			Y	FR II	Q	9	63
2253+417	J2255+4202	OY 489		Y		CT, CFS	Q		41, 42
2255+416	J2257+4154	4C 41.45		Y		CT, CSS	Q		41, 42
2311+469	J2313+4712	4C 46.47		Y		CT, CSS	Q		41, 42
2323+435	J2325+4346	S4 2323+43		Y		CSS	G	45	
2324+405	J2326+4048	3C 462		Y	Y	FR II	G (a)	9	19
2335+26	J2338+2701	3C 465			Y[b]	FR I	G	1,9	
2342+821	J2344+8226	S5 2342+82	Y		Y	CSS	Q (a)	9, 57, 56	
2351+456	J2354+4553	4C 45.51	Y		Y	U, CFS	Q (a)	9	31
2352+495	J2355+4950	DA 611	Y		Y	CSO	G		31, 75

Notes.

[a] M82 is not an active galaxy, and was therefore not included in the statistical analyses in this paper.

[b] Indicates objects in the PWS subsample (see the text).

[c] The references for the optical classes are as follows: we used the PW (Peacock & Wall 1981) optical identifications where available, otherwise the PR (Pearson & Readhead 1981) and CJ1 (Polatidis et al. 1995), where we replaced "SO" and "BL" entries with "Q." The only exceptions are from (a) Stickel et al. (1994) and (b) Peck & Taylor (2000). The columns are as follows: source names (1–3); membership in the PR, CJ1, and PW samples (4–6); source type (7): quasars (Q), galaxies (G), bona fide CSO (CSO), FR I, FR II, and FR?; objects unresolved by Peacock & Wall (1981) on the 5 km Telescope (U,CSS and U,CFS for CSS and compact flat spectrum sources, respectively); doubles identified by Peacock & Wall (1981) in which the optical ID coincides with one of the radio components (D2); CCS objects identified by Peacock & Wall (1981; CSS); objects found to be compact in various VLBI surveys other than any identified by Peacock & Wall (1981; CT, CSS or CT, CFS for CCS and compact flat spectrum sources, respectively); CSO catalog ID (8); optical identifications (9); and structure references (10–11). No attempt has been made at complete map references for each object since these number in the tens for many objects and the purpose of this table is solely to provide justification for the claim that the structures of all of these sources are well known.

References. (1) MacDonald et al. (1968); (2) Branson et al. (1972); (3) Pooley & Henbest (1974);(4) Riley & Pooley (1975); (5) Longair (1975); (6) Miley et al. (1975); (7) Bridle et al. (1976); (8) Jenkins et al. (1977); (9) Peacock & Wall (1981); (10) Cottrell (1977); (11) Waggett et al. (1977); (12) Fomalont et al. (1980); (13) Burns & Christiansen (1980); (14) Pearson & Readhead (1981); (15) Porcas (1981); (16) Kapahi (1981); (17) Laing (1981); (18) Birkinshaw et al. (1981); (19) Peacock & Wall (1982); (20) Laing et al. (1983); (21) Romney et al. (1984); (22) Owen & Puschell (1984); (23) Spangler et al. (1984); (24) Strom & Willis (1980); (25) Lonsdale (1984); (26) Jenkins (1982); (27) van Breugel & Fomalont (1984); (28) Fanti et al. (1986); (29) Leahy et al. (1986); (30) Alexander & Leahy (1987); (31) Pearson & Readhead (1988); (32) Bridle et al. (1989); (33) Pedlar et al. (1990); (34) Leahy & Perley (1991); (35) Altschuler et al. (1995); (36) Turland (1975); (37) Bridle et al. (1994); (38) Lister et al. (1994); (39) Giovannini et al. (1994); (40) Akujor et al. (1994); (41) Polatidis et al. (1995) or (Thakkar et al. 1995); (42) Xu et al. (1995); (43) Akujor & Garrington (1995); (44) Reid et al. (1995); (45) Sanghera et al. (1995); (46) Hardcastle et al. (1996); (47) Leahy et al. (1997); (48) Ludke et al. (1998); (49) Neff et al. (1995); (50) Dennett-Thorpe et al. (1999); (51) Fomalont et al. (2000); (52) Looney & Hardcastle (2000); (53) Saikia et al. (2001); (54) Dallacasa et al. (2013); (55) Thomasson et al. (2006); (56) Dallacasa et al. (1995); (57) Dallacasa et al. (2021); (58) MOJAVE website: https://www.cv.nrao.edu/MOJAVE/allsources.html; (59) Radio Fundamental Catalog (RFC); (60) Kellermann et al. (1998); (61) Giovannini et al. (2018); (62) Fernini (2014); (63) Akujor et al. (1991); (64) (Hardcastle et al. 1997); (65) Tremblay et al. (2016); (66) Baum et al. (1990); (67) Sokolovsky et al. (2011); (68) Altschuler et al. (1995); (69) Xu (1995); (70) Dallacasa et al. (1995); (71) Stanghellini et al. (2005); (72) Xiang et al. (2002); (73) Nagai et al. (2006); (74) Orienti & Dallacasa (2014); and (75) R96.

(This table is available in its entirety in machine-readable form.)

ORCID iDs

S. Kiehlmann https://orcid.org/0000-0001-6314-9177
A. C. S. Readhead https://orcid.org/0000-0001-9152-961X
M. L. Lister https://orcid.org/0000-0003-1315-3412
S. Bruzewski https://orcid.org/0000-0001-7887-1912
T. J. Pearson https://orcid.org/0000-0001-5213-6231
A. Siemiginowska https://orcid.org/0000-0002-0905-7375
K. Tassis https://orcid.org/0000-0002-8831-2038
G. B. Taylor https://orcid.org/0000-0001-6495-7731

References

Akujor, C. E., & Garrington, S. T. 1995, A&AS, 112, 235
Akujor, C. E., Luedke, E., Browne, I. W. A., et al. 1994, A&AS, 105, 247
Akujor, C. E., Spencer, R. E., Zhang, F. J., et al. 1991, MNRAS, 250, 215
Alexander, P., & Leahy, J. P. 1987, MNRAS, 225, 1
Altschuler, D. R., Gurvits, L. I., Alef, W., et al. 1995, A&AS, 114, 197
An, T., & Baan, W. A. 2012, ApJ, 760, 77
Augusto, P. 2009, AN, 330, 190
Augusto, P., Gonzalez-Serrano, J. I., Perez-Fournon, I., & Wilkinson, P. N. 2006, MNRAS, 368, 1411
Augusto, P., Wilkinson, P. N., & Browne, I. W. A. 1998, MNRAS, 299, 1159
Baum, S. A., O'Dea, C. P., Murphy, D. W., & de Bruyn, A. G. 1990, A&A, 232, 19
Birkinshaw, M., Laing, R. A., & Peacock, J. A. 1981, MNRAS, 197, 253
Blandford, R., Meier, D., & Readhead, A. 2019, ARA&A, 57, 467
Branson, N. J. B. A., Elsmore, B., Pooley, G. G., & Ryle, M. 1972, MNRAS, 156, 377
Bridle, A. H., Davis, M. M., Meloy, D. A., et al. 1976, Natur, 262, 179
Bridle, A. H., Fomalont, E. B., Byrd, G. G., & Valtonen, M. J. 1989, AJ, 97, 674
Bridle, A. H., Hough, D. H., Lonsdale, C. J., Burns, J. O., & Laing, R. A. 1994, AJ, 108, 766
Burns, J. O., & Christiansen, W. A. 1980, Natur, 287, 208
Callingham, J. R., Ekers, R. D., Gaensler, B. M., et al. 2017, ApJ, 836, 174
Carilli, C. L., Perley, R. A., Dreher, J. W., & Leahy, J. P. 1991, ApJ, 383, 554
Cohen, A. M., Porcas, R. W., Browne, I. W. A., Daintree, E. J., & Walsh, D. 1977, MmRAS, 84, 1
Cottrell, G. A. 1977, MNRAS, 178, 577
Curtis, H. D. 1918, PLicO, 13, 9
Dallacasa, D., Fanti, C., Fanti, R., Schilizzi, R. T., & Spencer, R. E. 1995, A&A, 295, 27
Dallacasa, D., Orienti, M., Fanti, C., & Fanti, R. 2021, MNRAS, 504, 2312
Dallacasa, D., Orienti, M., Fanti, C., Fanti, R., & Stanghellini, C. 2013, MNRAS, 433, 147
Dennett-Thorpe, J., Bridle, A. H., Laing, R. A., & Scheuer, P. A. G. 1999, MNRAS, 304, 271
Dent, W. A. 1965a, Sci, 148, 1458
Dent, W. A. 1965b, AJ, 70, 672
Fanaroff, B. L., & Riley, J. M. 1974, MNRAS, 167, 31P
Fanti, C., Fanti, R., Dallacasa, D., et al. 1995, A&A, 302, 317
Fanti, C., Fanti, R., de Ruiter, H. R., & Parma, P. 1986, A&AS, 65, 145
Fanti, C., Fanti, R., Parma, P., Schilizzi, R. T., & van Breugel, W. J. M. 1985, A&A, 143, 292
Fanti, R., Fanti, C., Schilizzi, R. T., et al. 1990, A&A, 231, 333
Fernini, I. 2014, ApJS, 212, 19
Fomalont, E. B., Frey, S., Paragi, Z., et al. 2000, ApJS, 131, 95
Fomalont, E. B., Palimaka, J. J., & Bridle, A. H. 1980, AJ, 85, 981
Förster Schreiber, N. M., & Wuyts, S. 2020, ARA&A, 58, 661
Giovannini, G., Feretti, L., Venturi, T., et al. 1994, ApJ, 435, 116
Giovannini, G., Savolainen, T., Orienti, M., et al. 2018, NatAs, 2, 472
Gregory, P. C., Scott, W. K., Douglas, K., & Condon, J. J. 1996, ApJS, 103, 427
Hardcastle, M. J., Alexander, P., Pooley, G. G., & Riley, J. M. 1996, MNRAS, 278, 273
Hardcastle, M. J., Alexander, P., Pooley, G. G., & Riley, J. M. 1997, MNRAS, 288, 859
Helmboldt, J. F., Taylor, G. B., Tremblay, S., et al. 2007, ApJ, 658, 203
Hubble, E. 1929a, PNAS, 15, 168
Hubble, E. 1929b, CoMtW, 3, 23
Jenkins, C. J., Pooley, G. G., & Riley, J. M. 1977, MmRAS, 84, 61
Jenkins, C. R. 1982, MNRAS, 200, 705
Kapahi, V. K. 1981, A&AS, 43, 381
Kellermann, K. I., & Pauliny-Toth, I. I. K. 1969, ApJL, 155, L71
Kellermann, K. I., Vermeulen, R. C., Zensus, J. A., & Cohen, M. H. 1998, AJ, 115, 1295
Kiehlmann, S., Lister, M. L., Readhead, A. C. S., et al. 2024, ApJ, 961, 240
Komatsu, E., Dunkley, J., Nolta, M. R., et al. 2009, ApJS, 180, 330
Kuehr, H., Pauliny-Toth, I. I. K., Witzel, A., & Schmidt, J. 1981, AJ, 86, 854
Lacy, M., Baum, S. A., Chandler, C. J., et al. 2020, PASP, 132, 035001
Laing, R. A. 1981, MNRAS, 195, 261
Laing, R. A., Riley, J. M., & Longair, M. S. 1983, MNRAS, 204, 151
Lawrence, C. R., Zucker, J. R., Readhead, A. C. S., et al. 1996, ApJS, 107, 541
Leahy, J. P., Black, A. R. S., Dennett-Thorpe, J., et al. 1997, MNRAS, 291, 20
Leahy, J. P., & Perley, R. A. 1991, AJ, 102, 537
Leahy, J. P., Pooley, G. G., & Riley, J. M. 1986, MNRAS, 222, 753
Lister, M. L., Aller, M. F., Aller, H. D., et al. 2018, ApJS, 234, 12
Lister, M. L., Gower, A. C., & Hutchings, J. B. 1994, AJ, 108, 821
Lister, M. L., Homan, D. C., Hovatta, T., et al. 2019, ApJ, 874, 43
Longair, M. S. 1975, MNRAS, 173, 309
Longair, M. S., & Scheuer, P. A. G. 1970, MNRAS, 151, 45
Lonsdale, C. J. 1984, MNRAS, 208, 545
Looney, L. W., & Hardcastle, M. J. 2000, ApJ, 534, 172
Ludke, E., Garrington, S. T., Spencer, R. E., et al. 1998, MNRAS, 299, 467
MacDonald, G. H., Kenderdine, S., & Neville, A. C. 1968, MNRAS, 138, 259
Miley, G. K., Wellington, K. J., & van der Laan, H. 1975, A&A, 38, 381
Minkowski, R. 1941, PASP, 53, 224
Nagai, H., Inoue, M., Asada, K., Kameno, S., & Doi, A. 2006, ApJ, 648, 148
Neff, S. G., Roberts, L., & Hutchings, J. B. 1995, ApJS, 99, 349
Nilsson, K., Valtonen, M. J., Kotilainen, J., & Jaakkola, T. 1993, ApJ, 413, 453
O'Dea, C. P., & Saikia, D. J. 2021, A&ARv, 29, 3
Orienti, M., & Dallacasa, D. 2014, MNRAS, 438, 463
Owen, F. N., & Puschell, J. J. 1984, AJ, 89, 932
Owsianik, I., & Conway, J. E. 1998, A&A, 337, 69
Owsianik, I., Conway, J. E., & Polatidis, A. G. 1999, NewAR, 43, 669
Pauliny-Toth, I. I. K. 1977, in IAU Symp. 74, Radio Astronomy and Cosmology, ed. D. L. Jauncey (Dordrecht: D. Reidel), 63
Pauliny-Toth, I. I. K., Witzel, A., Preuss, E., et al. 1978, AJ, 83, 451
Peacock, J. A., & Gull, S. F. 1981, MNRAS, 196, 611
Peacock, J. A., & Wall, J. V. 1981, MNRAS, 194, 331
Peacock, J. A., & Wall, J. V. 1982, MNRAS, 198, 843
Pearson, T. J., & Readhead, A. C. S. 1981, ApJ, 248, 61
Pearson, T. J., & Readhead, A. C. S. 1988, ApJ, 328, 114
Peck, A. B., & Taylor, G. B. 2000, ApJ, 534, 90
Pedlar, A., Ghataure, H. S., Davies, R. D., et al. 1990, MNRAS, 246, 477
Planck Collaboration, Aghanim, N., Akrami, Y., et al. 2020, A&A, 641, A6
Polatidis, A. G., Conway, J. E., Owsianik, I., et al. 2002, in 6th European VLBI Network Symposium on New Developments in VLBI Science and Technology, ed. E. Ros et al. (Bonn: Max-Planck-Institut für Radioastronomie), 139
Polatidis, A. G., Wilkinson, P. N., Xu, W., et al. 1995, ApJS, 98, 1
Pooley, G. G., & Henbest, S. N. 1974, MNRAS, 169, 477
Pooley, G. G., & Ryle, M. 1968, MNRAS, 139, 515
Porcas, R. W. 1981, Natur, 294, 47
Press, W. H., Flannery, B. P., Teukolsky, S. A., & Vetterling, W. T. 1992, Numerical Recipes in FORTRAN 77: The Art of Scientific Computing (2nd ed.; Cambridge: Cambridge Univ. Press)
Rawlings, S., & Saunders, R. 1991, Natur, 349, 138
Readhead, A. C. S. 1980, in IAU Symp. 92, Objects of High Redshift, ed. G. O. Abell & P. J. E. Peebles (Dordrecht: D, Reidel), 165
Readhead, A. C. S. 1994, ApJ, 426, 51
Readhead, A. C. S., Cohen, M. H., Pearson, T. J., & Wilkinson, P. N. 1978, Natur, 276, 768
Readhead, A. C. S., Kiehlmann, S., Lister, M. L., et al. 2021, AN, 342, 1185
Readhead, A. C. S., Ravi, V., Blandford, R. D., et al. 2024, ApJ, 961, 242
Readhead, A. C. S., Taylor, G. B., Xu, W., et al. 1996, ApJ, 460, 612
Readhead, A. C. S., Xu, W., Pearson, T. J., Wilkinson, P. N., & Polatidis, A. G. 1994, in Compact Extragalactic Radio Sources, ed. J. A. Zensus & K. I. Kellermann (Green Bank, WV: NRAO), 17
Rees, M. J. 1966, Natur, 211, 468
Rees, M. J. 1967, MNRAS, 135, 345
Reid, A., Shone, D. L., Akujor, C. E., et al. 1995, A&AS, 110, 213
Richards, J. L., Max-Moerbeck, W., Pavlidou, V., et al. 2011, ApJS, 194, 29
Riley, J. M., & Pooley, G. G. 1975, MmRAS, 80, 105
Romney, J., Padrielli, L., Bartel, N., et al. 1984, A&A, 135, 289
Saikia, D. J., Jeyakumar, S., Salter, C. J., et al. 2001, MNRAS, 321, 37
Sanghera, H. S., Saikia, D. J., Luedke, E., et al. 1995, A&A, 295, 629
Scheuer, P. A. G. 1995, MNRAS, 277, 331
Schmidt, M. 1968, ApJ, 151, 393

Scott, M. A., & Readhead, A. C. S. 1977, MNRAS, 180, 539
Slob, M. M., Callingham, J. R., Röttgering, H. J. A., et al. 2022, A&A, 668, A186
Sokolovsky, K. V., Kovalev, Y. Y., Pushkarev, A. B., Mimica, P., & Perucho, M. 2011, A&A, 535, A24
Spangler, S. R., Myers, S. T., & Pogge, J. J. 1984, AJ, 89, 1478
Spencer, R. E., Schilizzi, R. T., Fanti, C., et al. 1991, MNRAS, 250, 225
Stanghellini, C., Bondi, M., Dallacasa, D., et al. 1997, A&A, 318, 376
Stanghellini, C., O'Dea, C. P., Dallacasa, D., et al. 2005, A&A, 443, 891
Stickel, M., Meisenheimer, K., & Kuehr, H. 1994, A&AS, 105, 211
Strom, R. G., & Willis, A. G. 1980, A&A, 85, 36
Tacconi, L. J., Genzel, R., & Sternberg, A. 2020, ARA&A, 58, 157
Taylor, G. B., Readhead, A. C. S., & Pearson, T. J. 1996, ApJ, 463, 95
Thakkar, D. D., Xu, W., Readhead, A. C. S., et al. 1995, ApJS, 98, 33
Thomasson, P., Saikia, D. J., & Muxlow, T. W. B. 2006, MNRAS, 372, 1607
Tremblay, S. E., Taylor, G. B., Ortiz, A. A., et al. 2016, MNRAS, 459, 820
Turland, B. D. 1975, MNRAS, 172, 181
van Breugel, W., & Fomalont, E. B. 1984, ApJL, 282, L55
Verkhodanov, O. V., Trushkin, S. A., Andernach, H., & Chernenkov, V. N. 2005, BSAO, 58, 118
Waggett, P. C., Warner, P. J., & Baldwin, J. E. 1977, MNRAS, 181, 465
Wall, J. V., & Peacock, J. A. 1985, MNRAS, 216, 173
Wilkinson, P. N., Polatidis, A. G., Readhead, A. C. S., Xu, W., & Pearson, T. J. 1994, ApJL, 432, L87
Wilkinson, P. N., Readhead, A. C. S., Purcell, G. H., & Anderson, B. 1977, Natur, 269, 764
Xiang, L., Stanghellini, C., Dallacasa, D., & Haiyan, Z. 2002, A&A, 385, 768
Xu, W. 1995, PhD thesis, California Institute of Technology
Xu, W., Readhead, A. C. S., Pearson, T. J., Polatidis, A. G., & Wilkinson, P. N. 1995, ApJS, 99, 297